Open access • Journal Article • DOI:10.1038/NGEO3033

Methane bursts as a trigger for intermittent lake-forming climates on post-Noachian Mars — Source link

Edwin S. Kite, Peter Gao, Peter Gao, Colin Goldblatt ...+4 more authors

Institutions: University of Chicago, University of California, Berkeley, Ames Research Center, University of Victoria ...+3 more institutions

Published on: 01 Oct 2017 - Nature Geoscience (Nature Publishing Group)

Topics: Atmospheric methane, Methane clathrate, Mars Exploration Program, Methane and Noachian

Duration and rapid shutdown of Mars lake-forming climates explained by methane bursts

Edwin S. Kite[1,*], Colin Goldblatt[2], Peter Gao[3,4], David P. Mayer[1].
1. University of Chicago. 2. University of Victoria. 3. NASA Ames Research Center.
4. California Institute of Technology. (* kite@uchicago.edu).

Abstract.
Build-up of relatively young (≲3.6 Ga) deltas and alluvial fans on Mars required lakes to persist for >3 Kyr (assuming dilute flow), but the watersheds' little-weathered soils indicate a climate history that was >99% dry. The lake-forming climates' trigger mechanism remains unknown. Here we show that these intermittency constraints, while inconsistent with many previously-proposed triggers for lake-forming climates, are consistent with a novel CH_4-burst mechanism. Chaotic transitions in mean obliquity drive latitudinal shifts in temperature and ice loading that destabilize CH_4 clathrate. For past clathrate hydrate stability zone occupancy fractions ≳0.2, we show that CH_4(±C_2H_6) builds up to levels whose radiative forcing (>15 W/m^2, plus feedbacks) is sufficient to modulate lake-forming climates. Such occupancy fractions are consistent with CH_4+C_2H_6 production by >3 Ga water-rock reactions. Sub-lake CH_4 destabilization provides positive feedback. UV-limited CH_4 photolysis curtails individual lake-forming climates to <10^6 yr duration, consistent with data. Our results show how a warmer early Mars can undergo intermittent excursions to a warm, wet climate state.

Introduction.
Runoff on Mars after ~3.6 Ga was uncommon and episodic. Episodes of runoff are recorded by deltas and fans. Fan/delta watershed mineralogy shows limited aqueous weathering, and watershed topography lacks the slope-area scaling expected for prolonged fluvial erosion. Both observations suggest runoff episodes were brief. Yet surprisingly, sediment and water mass balance calculations for ≲3.6 Ga precipitation-fed paleolakes do not suggest a palimpsest of catastrophic events. To the contrary, runoff production of ~0.15 mm/hr and lake lifetimes of >3 Kyr (assuming dilute flow) requires sustained, non-catastrophic cycling of lake-water (e.g. Irwin et al. 2015, Palucis et al. 2016, Williams & Weitz 2014) (Table S1). Catchments lack evidence for surface weathering, and retain mafic minerals such as olivine, which dissolves quickly in water (e.g. Milliken & Bish 2010; SI). Furthermore, late-stage fluvial incision into delta and fan deposits is uncommon. In summary, individual lake-forming climates lasted >3 Kyr but shut down rapidly.

To draw out the implications of the intermittency data, we use a conceptual model of catchment response to a ~3 Ga wet episode (Fig. 1a). Consistent with models (e.g. Mischna et al. 2013), we assume snow falls in low-latitude catchments when obliquity (φ) >40°. During climate optimum, runoff from snowmelt transports sediment to build a fan/delta. This phase lasts >(3-10) Kyr (the product of delta volume V and water:sediment ratio, divided by the energy-limited lake evaporation

rate – Irwin et al. 2015, Williams & Weitz 2014, Palucis et al. 2016) (Table S1). During this phase, erosion exposes mafic minerals (e.g. olivine) in sediment-source regions (Fig. 1a). As climate cools, meltwater production is insufficient to transport sediment, but still wets the active-layer soil and so dissolves olivine. The duration of this phase cannot exceed the olivine-dissolution lifetime, $\sim 10^6$ yr (Stopar et al. 2006, Olsen & Rimstidt 2007). The surface-energy-balance requirements for delta-building and soil-wetting are separated by ≥15 W/m^2 (the energy cost of producing enough runoff to match paleodischarge constraints) (SI). The total interval over which all $\lesssim$3.6 Ga lake-forming climates occurred is unknown. However, many sites show evidence for 2-3 fluvial sediment transport pulses.

Hypotheses for the trigger of lake-forming climates should match constraints on the intermittency and cadence of those climates. Many existing hypotheses for the trigger of lake-forming climates fail the lake-duration test (Fig. 1b). Volcanic forcing predicts individually-brief wet events (Halevy & Head 2014, Kerber et al. 2015). Models of $\sim$3 Ga asteroid impacts predict <0.1 yr runoff (Segura et al. 2013). A H_2-CO_2 greenhouse requires >1 bar atmosphere and requires >0.4 Myr to remove H_2 at the diffusion-limited rate (Ramirez et al. 2014); this is marginally consistent with data, but requires a brief >10^7 km^3 pulse of late-stage volcanism (or clathrate release; Chassefière et al. 2016) and an efficient late-stage CO_2-removal mechanism.

An alternative trigger for lake-forming climates is chaotic transitions in Mars' mean obliquity. These transitions are large (10-20°), brief (often $\lesssim 10^7$ yr), and infrequent: transported to a random point in Mars' history, one would expect to find oneself in a 0.5 Gyr-long interval of continuously high (or low) Myr-mean φ (Fig. 2). The brevity and large time interval of mean-φ transitions matches the brevity and rarity of lake-forming climates. Moreover, mean-φ transitions cause latitudinal shifts in temperature, which destabilizes ice/snow (e.g., Mischna et al. 2013). Thus φ shifts increase the amount of water in the atmosphere, favor cirrus-cloud warming (Urata & Toon 2013), and prime the system for melting (Mischna et al. 2013).

During an increase (or decrease) in mean φ, the high-latitude (or low-latitude) subsurface will decompress (as surface ice and ground ice migrates) and warm. This destabilizes CH_4-clathrate, yielding CH_4 gas (Root & Elwood-Madden 2012). CH_4/C_2H_6 is produced as a consequence of hydrothermal circulation (e.g. serpentinization) early in Mars history (e.g. Lyons et al. 2005), and forms clathrate on approach to a cold surface. CH_4-clathrate breakdown involves a >14% reduction in solid volume, and we assume fractures allow methane gas released at ≤100m depth to reach the surface in $\ll 10^5$ yr. The stoichiometric upper limit on CH_4 produced by serpentinization is >3000 × greater than the amount needed to shift planetary climate. Methane-saturated fluids will deposit clathrate on approach to a cold surface. As Mars cools, the clathrate hydrate stability zone (CHSZ) expands. Methane will diffuse out of clathrate only slowly, but once destabilized, CH_4-clathrate dissociates geologically quickly (Root & Elwood-Madden 2012).

Mean-φ transitions can lead to build-up of millibars of methane in Mars' atmosphere. To show this, we used calculations of Mars' spin and orbit to drive a 2D model of methane stability in Mars' subsurface. Because our interest is in the depth to the top of the CHSZ, we ignored temperature-conductivity feedback. We used mobile ice+dust overburden of ~40 m thickness (e.g. Kadish et al. 2010). The fraction *f* of pore space in the CHSZ that is occupied by hydrate is a free parameter. Example output is shown in Fig. 4. Following model spinup, little happens for ~0.3 Gyr. The CHSZ will deepen as solar luminosity increases, but CH_4 released to the atmosphere during quasi-periodic orbital change (Prieto-Ballesteros et al. 2006) is maintained below radiatively significant levels by Ly-α photolysis (Krasnopolsky et al. 2004). Then, a mean-φ shift occurs, swiftly destabilizing CH_4-clathrate (Fig. 4). CH_4 release temporarily overwhelms photolysis by Ly-α (we use a ~3.3 Ga UV flux; Güdel 2007); CH_4 accumulates in the atmosphere. Assuming photon-limited CH_4 destruction, the Mars atmosphere CH_4-enrichment episode lasts $f \times 10^6$ years. This allows for multiple orbitally-paced pulses of runoff in a single lake-forming climate episode, consistent with data (Williams & Weitz 2014), and satisfies the lake-duration constraint. A stepwise change in obliquity can elicit multiple episodes separated by 1-50 Myr. However, the CH_4-clathrate reservoir is recharged slowly if at all, so the CH_4-burst mechanism satisfies the olivine-dissolution constraint.

Millibars of methane can switch the Mars system from zero meltwater production to a lake-forming climate. Assuming a surface initially just below the melting point and an isothermal stratosphere, 1 mbar of CH_4 added to a 100 mbar CO_2 atmosphere in a clear-sky radiative column calculation boosts tropopause energy balance by 14 W/m^2 (see Supplementary information; also Byrne & Goldblatt, 2014). For <100 mbar CO_2, the effect is enhanced. The preference for thin atmospheres is not strong however, because for higher pressures, CH_4-CO_2 collision-induced absorption (which is not included in our model) provides an alternative mechanism for CH_4-driven warming (Wordsworth et al. 2016). The likely presence of clouds would moderate total warming, but only by 14-30% (Goldblatt & Zahnle 2011). Our calculations assume NIR absorbed in the planetary boundary layer contributes to surface warming (Byrne & Goldblatt 2014). C_2H_6 is produced in the subsurface alongside CH_4 at 0.1-10% levels (Etiope & Sherwood-Lollar 2013) and partitions readily into clathrate (Sloan & Koh 2008). A 10% C_2H_6/CH_4 release ratio would give 35 W/m^2 warming (Fig. 3), and even a 1% C_2H_6/CH_4 would be radiatively significant (Haqq-Misra et al. 2008). C_2H_6 promotes dissociation of CH_4 clathrate at lower pressure, and the response of mixed CH_4/C_2H_6 clathrate to orbital change is qualitatively similar to that of CH_4. We show results for $CH_4/CO_2 \leq 0.1$, for which photochemical production of C_2H_6 is minor and antigreenhouse haze cannot form. Runoff production (0.15-0.35 mm/hr) is sufficient to match paleodischarge constraints, even without feedbacks.

Net positive feedbacks are likely and would boost CH_4-induced warming. Water vapor and perhaps cloud feedbacks boost warming (e.g. Mischna et al. 2013). For the portion of the surface that is submerged during a lake-forming event, lake-bottom temperature rises to ~277K even for ice-covered lakes. This warming

destabilizes sub-lake clathrates. The largest certain paleolake on Mars is 10^6 km^2 (Irwin et al. 2002). Release of CH_4 from destabilized clathrate beneath this paleolake (e.g. via mud volcanoes) doubles atmospheric CH_4 (Fig. 3). This talik feedback extends lake lifetime in proportion to lake area. Seas as large as 2.3×10^7 km^2 have been suggested (Carr & Head 2003). Large paleolakes at ~3.8 Ga may have both resulted from and also permitted more persistent runoff at that time.

Mean-φ transitions could drive also lake-forming climate by linking surface and subsurface hydrology (Baker et al. 1991). For example, ice unloading could promote hydrofracture discharge of overpressured aquifers. Pooling of floodwaters could then engage the talik feedback. Clathrate decomposition, e.g. driven by φ changes, might directly trigger outflow channels (Baker et al. 1991).

Because widely-spaced CH_4 bursts are possible, we hypothesize that the ~3 Ga lake-forming climate may be a late echo of the more-intense ~4 Ga climate upswing that cut valley networks and filled inland seas (Irwin et al. 2005). For example, atmospheric collapse could drive ice sheets from highlands to poles (Wordsworth et al. 2015), depressurizing sub-ice clathrate. Conversely, >5 widely-separated lake episodes would be inexplicable by CH_4 bursts alone.

In our model, surface climate ~3 Ga is driven by CH_4 produced during earlier water-rock reactions. Orbiter data show that serpentinization did occur (Ehlmann et al. 2010), and suggest cool mid-crustal temperatures that are consistent with pervasive hydrothermal circulation and a cold surface. Better constraints on permeability, alteration extent, and fluid chemistry in ancient deep aquifers could test for the abundant CH_4 predicted by our model (Saper & Mustard 2013). The CH_4-clathrate reservoir on Mars should never completely vanish. Present-day CH_4 outgassing is predicted (Chassefière & Leblanc, 2011). CH_4 outgassing has been reported from ground-based and rover instruments (e.g. Webster et al. 2015). Our model indicates that ancient clathrate should be closest to the surface in dusty longitudes at 30-50°N. The 2016 ExoMars orbiter will decisively test modern outgassing (Vandaele et al. 2015). If CH_4/CO_2 exceeded ~0.1, organic haze would be produced and complex (but abiotic) organic matter would be preferentially incorporated into paleolake sediments.

Our model of the anomalies – the wettest climates – on ~3 Ga Mars assumes a base state warmer than the present (e.g. Urata & Toon 2013). Otherwise, a CH_4 burst would struggle to explain the runoff data. A warmer base state may also be required to explain the prolonged accumulation of sedimentary rocks near Mars' equator (e.g. Malin & Edgett 2000). While CH_4/C_2H_6 bursts can explain the cadence of lake-forming climates superimposed on a warmer base state, the problem of accounting for a warmer base state remains open (Wordsworth et al. 2015).

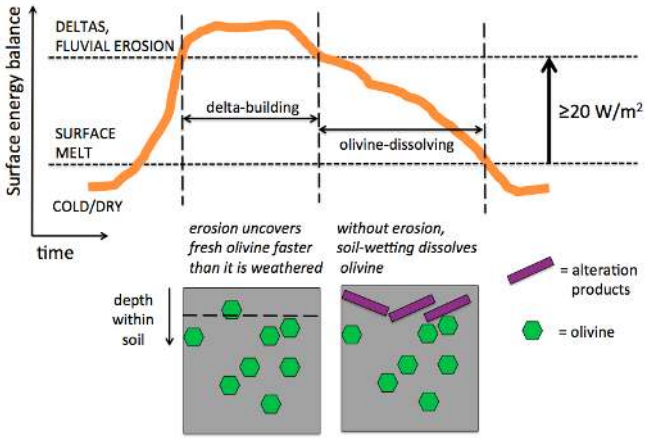

(a)

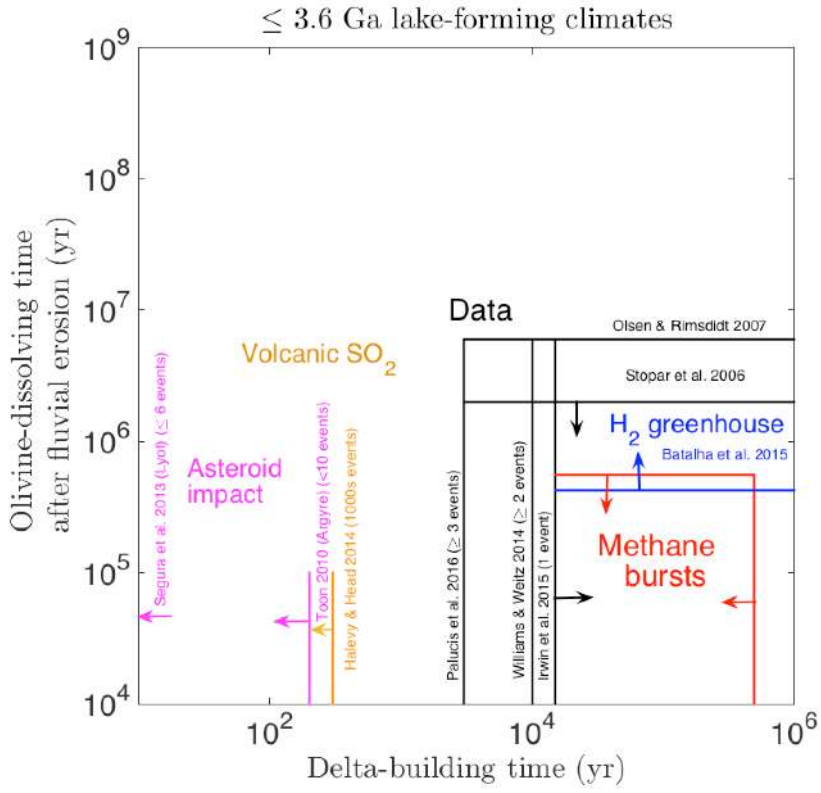

(b)

Fig. 1. (a) Schematic showing how the delta-building constraint and the olivine-preservation constraint constrain duration and shutdown-time for a lake-forming climate episode. Olivine constrains soil-wetting after fluvial erosion ceases. (b) Geologic constraints on the duration and shutdown-speed of lake-forming climates (green) compared to models for the trigger mechanism of lake-forming climates (colors). For CH_4 bursts, Results are plotted for $f < 0.3$ (see text).

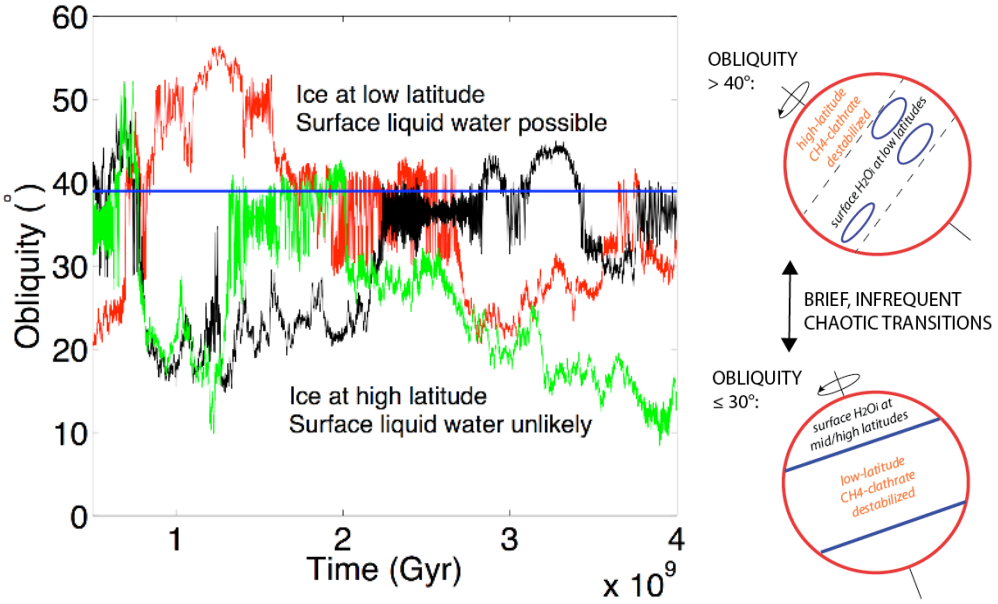

Fig. 2. *Left:* Examples of possible orbital histories for Mars. *Right:* Schematic showing effect of obliquity change on surface-ice distribution.

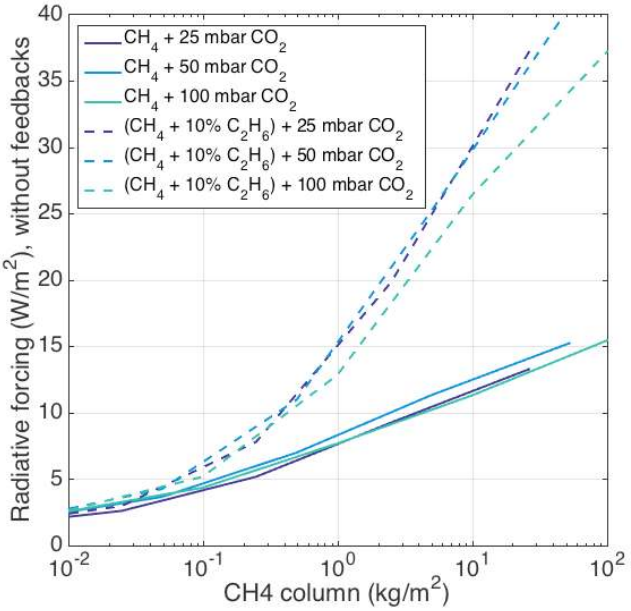

Fig. 3. Net CH_4 (and CH_4 + C_2H_6) radiative forcing at the tropopause for a surface temperature initially just below the freezing point, combining stratospheric solar absorption and longwave forcing. The x-axis is shown in column mass of CH_4 so that equal amounts are compared; 1 kg/m^2 corresponds to CH4 mixing ratios of (2×10^{-3} , 1×10^{-3}) for 50 and 100mbar of CO_2. Clear-sky; no feedbacks are included. CO_2-CH_4 collision-induced absorption (not included) can also boost warming (Wordsworth et al. 2016).

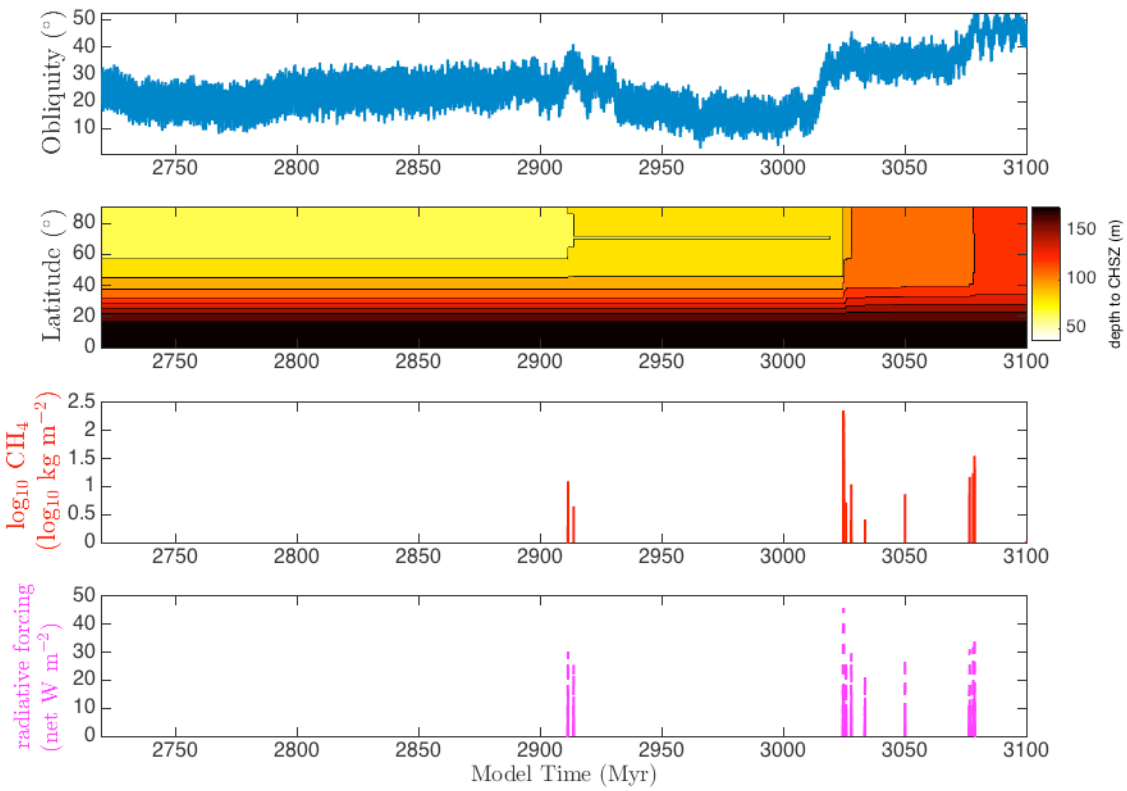

Fig. 4. Triggering of a CH_4-enabled lake-forming climate on Mars. Individual lake-forming events last 10-300 Kyr (Fig. S6a). (a) Example obliquity forcing (preceded by 0.3 Gyr of continuously low obliquity). (b) Depth to the top of the clathrate-hydrate stability zone. Darkening of colors indicates clathrate destabilization. (c) Atmospheric CH_4 column mass (f = 0.5). Dashed line includes talik feedback. (d) Radiative forcing, without any climate feedbacks. Solid line is for CH_4 alone; dashed line is for CH_4+10%C_2H_6.

Acknowledgements. We thank J.C. Armstrong, R.M.E. Williams, T. Onstott, A.D. Howard, R.P. Irwin III, M. Palucis, M. Mischna, V. Hamilton, D. Stolper, B. Ehlmann, and D. Archer. We acknowledge UChicago's Research Computing Center and NASA funding (NNX16AG55G+NNX15AM49G).

References.

Armstrong, J.C., Leovy, C.B., Quinn, T. 2004. A 1 Gyr climate model for Mars: new orbital statistics and the importance of seasonally resolved polar processes. Icarus 171, 255-271.

Baker, V.R., Strom, R.G., Gulick, V.C., Kargel, J.S., Komatsu, G. 1991. Ancient oceans, ice sheets and the hydrological cycle on Mars. Nature 352, 589-594.

Byrne, B., Goldblatt, C. 2014. Radiative forcings for 28 potential Archean greenhouse gases. Climate of the Past 10, 1779-1801.

Carr, M.H., Head, J.W. 2003. Oceans on Mars: An assessment of the observational evidence and possible fate. JGR (Planets) 108, 5042-1.

Chambers, J.E. 1999. A hybrid symplectic integrator that permits close encounters between massive bodies. Monthly Notices of the Royal Astron. Soc. 304, 793-799.

Chassefière, E., Leblanc, F. 2011. Methane release and the carbon cycle on Mars. Planet. & Space Sci. 59, 207-217.

Chassefière, E., Lasue, J., Langlais, B., Quesnel, Y. 2016. Early Mars Serpentinization Derived CH_4 Reservoirs and H_2 Induced Warming. Meteoritics & Planetary Science, doi:10.1111/maps.12784.

Ehlmann, B.L., Mustard, J.F., Murchie, S.L. 2010. Geologic setting of serpentine deposits on Mars. GRL 37, L06201.

Goldblatt, C.; Zahnle, K. J., 2011, Clouds and the Faint Young Sun Paradox, Climate of the Past, 7, 1, 203-220.

Güdel, M. 2007. The Sun in Time: Activity and Environment. Living Reviews in Solar Physics 4.

Halevy, I., Head, J.W., III 2014. Episodic warming of early Mars by punctuated volcanism. Nature Geoscience 7, 865-868.

Haqq-Misra, J.D., Domagal-Goldman, S.D., Kasting, P.J., Kasting, J.F., 2008, A Revised, Hazy Methane Greenhouse for the Archean Earth. Astrobiology 8, 1127-1137.

Irwin, R.P., Lewis, K.W., Howard, A.D., Grant, J.A. 2015. Paleohydrology of Eberswalde crater, Mars. Geomorphology 240, 83-101.

Irwin, R.P., Maxwell, T.A., Howard, A.D., Craddock, R.A., Leverington, D.W. 2002. A Large Paleolake Basin at the Head of Ma'adim Vallis, Mars. Science 296, 2209-2212.

Irwin, R.; Howard, A.; Craddock, R.; Moore, J., 2005, An intense terminal epoch of widespread fluvial activity on early Mars: 2. Increased runoff and paleolake development, J. Geophys. Res., 110, E12S15.

Kadish, S.J., Head, J.W., Barlow, N.G. 2010. Pedestal crater heights on Mars: A proxy for the thicknesses of past, ice-rich, Amazonian deposits. Icarus 210, 92-101.

Kerber, L., Forget, F., Wordsworth, R. 2015. Sulfur in the early martian atmosphere revisited: Experiments with a 3-D Global Climate Model. Icarus 261, 133-148.

Krasnopolsky, V.A., Maillard, J.P., Owen, T.C. 2004. Detection of methane in the martian atmosphere: evidence for life?, Icarus 172, 537-547.

Laskar, J., Correia, A.C.M., Gastineau, M., Joutel, F., Levrard, B., Robutel, P. 2004. Long term evolution and chaotic diffusion of the insolation quantities of Mars. Icarus 170, 343-364.

Lyons, J.R., Manning, C., Nimmo, F. 2005. Formation of methane on Mars by fluid-rock interaction in the crust. GRL 32, L13201.

Malin, M.C., Edgett, K.S. 2000. Sedimentary Rocks of Early Mars. Science 290, 1927-1937.

Milliken, R.E., Bish, D.L. 2010. Sources and sinks of clay minerals on Mars. Philosophical Magazine 90, 2293-2308.

Mischna, M.A., Baker, V., Milliken, R., Richardson, M., Lee, C. 2013. Effects of obliquity and water vapor/trace gas greenhouses in the early martian climate. JGR (Planets) 118, 560-576.

Olsen, A.A., & Rimstidt, J.D., 2007, Using a mineral lifetime diagram to evaluate the persistence of olivine on Mars, American Mineralogist, 92, 4, 598–602.

Palucis, M.C., Dietrich, W.E., Williams, R.M.E., Hayes, A.G., Parker, T., Sumner, D.Y., Mangold, N., Lewis, K., Newsom, H. 2016. Sequence and relative timing of large lakes in Gale crater (Mars) after the formation of Mount Sharp. JGR (Planets) 121, 472-496.

Prieto-Ballesteros, O., Kargel, J.S., Fairén, A.G., Fernández-Remolar, D.C., Dohm, J.M., Amils, R. 2006. Interglacial clathrate destabilization on Mars: Possible contributing source of its atmospheric methane. Geology 34, 149.

Root, M.J., Elwood Madden, M.E. 2012. Potential effects of obliquity change on gas hydrate stability zones on Mars. Icarus 218, 534-544.

Saper, L., Mustard, J.F. 2013. Extensive linear ridge networks in Nili Fossae and Nilosyrtis, Mars: implications for fluid flow in the ancient crust, GRL 40, 245-249.

Segura, T.L., Zahnle, K., Toon, O.B., McKay, C.P. 2013, pp. 417-437 *in* Mackwell, S., et al. (Eds). Comparative Climatology of Terrestrial Planets, University of Arizona Press.

Stopar, J.D., Jeffrey Taylor, G., Hamilton, V.E., Browning, L. 2006. Kinetic model of olivine dissolution and extent of aqueous alteration on mars. Geochimica et Cosmochimica Acta 70, 6136-6152.

Urata, R.A., Toon, O.B. 2013. Simulations of the martian hydrologic cycle with a general circulation model: Implications for the ancient martian climate. Icarus 226, 229-250.

Vandaele, A.C., and 42 colleagues, 2015. Science objectives and performances of NOMAD, a spectrometer suite for the ExoMars TGO mission. Planetary and Space Science 119, 233-249.

Webster, C.R., and 569 colleagues 2015. Mars methane detection and variability at Gale crater. Science 347, 415-417.

Williams, R.M.E., Weitz, C.M. 2014. Reconstructing the aqueous history within the southwestern Melas basin, Mars: Clues from stratigraphic and morphometric analyses of fans. Icarus 242, 19-37.

Wordsworth, R., Kalugina, Y., Lokshtanov, S., Vigasin, A., Ehlmann, B., Head, J., Sanders, C. and Wang, H. 2016, Transient reducing greenhouse warming on early Mars, arXiv:1610.09697v1.

Wordsworth, R.; Kerber, L.; Pierrehumbert, R.; Forget, F.; Head, J.W., 2015, Comparison of warm and wet and cold and icy scenarios for early Mars in a 3-D climate model, JGR: Planets, 120, 1201-1219.

Supplementary Information.

This Supplementary Information contains (Section 1) details of the geologic analysis, and (Section 2) details of the methods used.

1. Supplementary Geological Analysis.

Deltas/fans. For many low-latitude fluviolacustrine deposits on Mars, crosscutting relationships, crater counts, and relative preservation state all suggest a mid-Hesperian to Early Amazonian age (e.g., Mangold et al. 2004, Warner et al. 2010, Palucis et al. 2016, Williams & Weitz 2014, Mangold et al. 2012, Irwin et al. 2015, Grant et al. 2011, Fassett & Head 2008, Grant et al. 2014, Howard & Moore 2011, Wilson et al. 2016). This corresponds to ~3 Ga using Werner & Tanaka's (2011) chronology (or ~2 Ga using the alternative chronology of Robbins, 2014). These deposits postdate the highland valley networks of Mars, which formed ~3.8 Ga (Fassett & Head 2008). They are usually also better preserved than the ~3.8 Ga landforms. Published data are consistent with the globally-distributed deposits having been caused by 1-2 intervals of delta-building, each occupying a small fraction of the total time spanned by the Late Hesperian and Early Amazonian. At some locations this interval was apparently divided into multiple wet-dry pulses (Irwin et al. 2015, Williams & Weitz 2014).

Precipitation (rain or snowmelt) is the water source for the fans and deltas considered in this paper. Their spatially clustered watersheds show channels extending near ridgelines (Grant & Wilson 2012). Seasonal melting is a reasonable hypothesis for ~3 Ga deposits, although the reasoning set out in this paper does not rule out rainfall. Other ~3 Ga paleochannels and fluvial deposits (not considered in this paper) are more ambiguous, and might be formed either by precipitation runoff (Lamb et al. 2008, Adeli et al. 2016) or alternatively by spring discharge, jökulhlaups, or impact-triggered processes (Hauber et al. 2013, Williams & Malin 2008, Kite et al. 2011a).

The delta-forming duration τ_1 (the duration of fluvial sediment transport) must exceed

$$\tau_1 > V_d(V_w/V_s)/EA_p \qquad (1)$$

where V_d (m^3) is the measured delta volume, V_w/V_s is the water:sediment ratio, E (m yr^{-1}) is the evaporation rate (constrained by energy balance), and A_p (m^2) is lake area (Irwin et al. 2015, Palucis et al. 2016) (Table S1). Energy balance limits evaporation rate to <1 m yr^{-1} (Irwin et al. 2015). Deposit morphology strongly suggests dilute flows (debris-flow deposits are seen, but are uncommon; e.g. Williams et al. 2011). Most authors therefore assume a dilute V_w/V_s ratio ≥ 10^3, consistent with Earth data (e.g. Syvitski et al. 2003). The long minimum lake lifetimes inferred from delta volumes are consistent with minimum runoff durations

calculated from the energy-balance limit on runoff production (Kite et al. 2013) combined with alluvial-fan volumes (Williams et al. 2011). Because the water demands (column meters) of both deltas and alluvial-fans exceed the plausible thickness of preexisting snowpack, precipitation must have continued during the wet event. This implies a hydrologic cycle.

Site	Delta volume (V_d, km^3)	Lake area (A_p, km^2)	Evaporation rate constraint (E, m/yr)	V_W/V_S assumed	Minimum lake lifetime (Kyr)
Eberswalde delta (1)	6	>410	<1 m/yr	10^3	15
SW Melas Fan "C" (2)	3.5	350	<1 m/yr	10^3	10
SW Melas Fan "F" (2)	1.3	350	<1 m/yr		4
Dulce Vallis (3)	1.5	3008	<1 m/yr	10^3	0.5
Farah Vallis (4)	22.5	3617	<1 m/yr	10^3	6
Gale Pancake(3)	14	5832	<1 m/yr	10^3	3

Sources of measurements: 1. Irwin et al. 2015. 2. Williams & Weitz 2014. 3. Palucis et al. 2016.

Table S1. Minimum paleolake lifetimes. We used published delta volume and lake area data, and applied a uniform lake evaporation rate and sediment:water ratio. Infiltration was neglected.

Assuming runoff from snowmelt, the runoff rate is directly related to the surface energy balance. The surface energy balance difference J (W/m^2) between the energetic threshold for soil wetting (no runoff), and the same threshold for fluvial sediment transport, is

$$J = \rho L(Q/A + I + E_e) \qquad (2)$$

where ρ is liquid water density (1000 kg m^{-3}), L is the latent heat of melting snow/ice (334 kJ kg^{-1}), Q is river paleodischarge (m^3 s^{-1}), A is the drainage area in m^2 (Q/A is "runoff production"), I is infiltration rate (mm hr^{-1}), and E_e is the excess evaporation (mm hr^{-1}). A lower bound on J is obtained by setting I and E_e to zero; then $J = \rho LQ/A$. For $\lesssim$3.6 Ga precipitation-fed channels, Q/A is estimated as ~0.1–0.2 mm hr^{-1} for Saheki (Morgan et al. 2014), 0.03 – 0.4 mm hr^{-1} for Peace Vallis (Palucis et al. 2014 as updated by Dietrich et al. accepted), and 0.1-0.3 mm hr^{-1} for Eberswalde (Irwin et al. 2015). We take 0.15 mm hr^{-1} as representative. For Q/A = 0.15 mm hr^{-1}, J = 15 W m^{-2}.

Unlike rivers on Earth, the Mars valley networks (where measured) do not modify the landscape sufficiently for river-channel topography to match terrestrial slope-area relationships (Aharonson et al. 2002, Som et al. 2009). Knickpoints are also

pervasive for ~3 Ga valley networks (e.g., Irwin et al. 2015). Therefore, the rivers of Mars flowed for a shorter time than the rivers of Earth, or the rivers of Mars were less effective than the rivers of Earth at eroding their substrate, or both. The timescale for Mars alluvial-fan catchments to approach topographic equilibrium is approximately 0.25-20 Myr (Armitage et al. 2011).

Although we focus on ≲3.6 Ga lake-forming climate(s), the ~4 Ga lake-forming climate is also characterized by a relatively short-lived interval of intense fluvial sediment transport (Irwin et al. 2005, Barnhart et al. 2009, Matsubara et al. 2013; but see also Hoke & Hynek 2009).

Olivine persistence. Olivine is present in many (perhaps all) Mars delta and alluvial-fan watersheds. Specifically, (1) olivine is detected by the Mars Express Observatoire pour la Minéralogie, l'Eau, les Glaces et l'Activité (OMEGA) (Ody et al. 2013) in some alluvial fan watersheds. (2) Olivine is widespread in Mars Global Surveyor Thermal Emission Spectrometer (TES) data (Koeppen & Hamilton 2008) including in alluvial fan watersheds. (3) Decorrelation stretches of Mars Odyssey Thermal Emission Imaging System (THEMIS) bands 9, 7 and 5 (Hamilton & Christensen 2005) indicate olivine in many locations, including alluvial fan watersheds. (4) The Mars Reconnaissance Orbiter Compact Reconnaissance Imaging Spectrometer for Mars (CRISM) OLINDEX3 parameter, which was designed as an indicator of olivine (Viviano-Beck et al. 2014), shows high values in many alluvial fan watersheds. Olivine detections in alluvial-fan watersheds using CRISM spectra include Robert Sharp (Buz & Ehlmann 2015) and Saheki (Fig. S1).

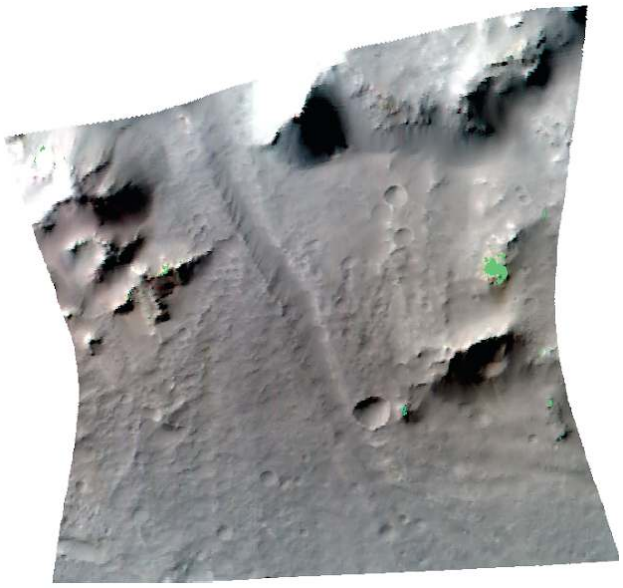

Figure S1. An olivine outcrop in an alluvial fan source region (fan drains to bottom of image). Olivine detections highlighted in green. Spectra for individual pixels within these areas were checked manually in order to verify that absorptions diagnostic of olivine were present. CRISM FRT00016E79, Saheki crater.

Olivine persistence sets an upper limit on the duration of soil wetting by olivine-dissolving fluids. Olivine-dissolution data indicate olivine lifetimes <2-6 Myr for T~278 K, for pH equilibrated with 60 mbar CO_2, and including a 100× lab-to-field correction (Stopar et al. 2006, Olsen & Rimsdidt 2007). Some calculations give olivine lifetimes in fluids at Mars' surface as short as 10 yr (Hurowitz & Mclennan 2007). Olivine-inferred water durations are consistent with short water durations inferred from the persistence of hydrated amorphous silica (Tosca & Knoll 2009), from reaction-transport model calculations (Berger et al. 2009), from the persistence of jarosite (Elwood-Madden et al. 2009), and from near-isochemical alteration of Bradbury Formation materials at Gale crater (McLennan et al. 2014).

We assume that infiltrated water is present in soil throughout a wet season. This is reasonable because runoff generation from snowpack is extremely difficult unless the snowpack reaches thermal maturity. Thermal maturity requires that average temperature during the warm month is comparable to the freezing point (Woo 2012). Additionally, infiltration into the deeper part of the soil, and the latent heat released from partial freezing, protect the water from complete freezing.

Ice/snow distribution with φ. Snow accumulation at latitude <45° at φ>40° (for atmospheric pressure $\lesssim$ 100 mbar) is supported by all climate models (e.g. Forget et al. 2006, Kite et al. 2013, Mischna et al. 2013). Snow accumulation at latitude <45° at φ>40° is also supported by observations of equatorial relict ice and glacial moraines (e.g., Shean 2010). This latitudinal shift in snow distribution is driven by high polar summer solstice temperatures at high obliquity. Because annual-mean sublimation losses at the poles exceed sublimation losses at low latitudes, snow/ice migrates to the low-latitude cold-trap. At high atmospheric pressure, snow/ice will be present at low latitudes regardless of φ (Wordsworth et al. 2015).

The thickness of outliers of past mantling layers indicates that Amazonian laterally-extensive midlatitude volatile-rich layers that migrate under φ control are (32-44)m thick (Kadish et al. 2010, Skinner et al. 2012). We take this to be representative of the Late Hesperian – Early Amazonian thickness. Loss of water over time (Mahaffy et al. 2015) implies that Late Hesperian volatile-rich layers would be even thicker than Amazonian volatile-rich layers. Because unloading of a thick layer would produce a stronger CH_4 burst, this strengthens our conclusions.

Previously-proposed trigger mechanisms.

- Volcanic SO_2: The SO_2-greenhouse model of Halevy & Head (2014) predicts wet events of duration ~30 yr. Because many volcanic eruptions have occurred on Mars, volcanic-greenhouse models predicts >100 wet events over a >10^8-yr interval. This hypothesis cannot match the minimum lake lifetime constraint, unless the lake level rose and fell repeatedly without leaving geologic signatures that can be recognized in a HiRISE image. Kerber et al. (2015) suggest that the wet-event duration for an SO_2-greenhouse is likely shorter than in the model of Halevy & Head (2014).

- H_2-boosted CO_2 greenhouse: A H_2-CO_2 greenhouse requires >1 bar atmosphere and requires >0.4 Myr to remove 10% H_2 (by volume) from a 2.5 bar CO_2-dominated atmosphere at the diffusion-limited rate (Ramirez et al. 2014). This is marginally consistent with data, but requires a <1 Myr duration $>10^7$ km^3 pulse of late-stage volcanism and an efficient late-stage CO_2-removal mechanism.
- Impacts: Impact-triggered models for post-3.6 Ga wet climates must satisfy the geologic constraint of modest precipitation-sourced erosional modification of the six largest post-3.6 Ga craters on Mars (Irwin 2013). Urata & Toon (2013) propose a metastable impact-triggered wet climate sustained by cloud forcing. The end of the climate would be driven by loss of water, e.g. by hydrogen escape. Ramirez & Kasting (2016) find that such a climate can sustain temperatures above 273K on annual average, but only with unrealistic total cloud cover. However, the model could generate seasonal melting with more realistic cloud-cover assumptions. Segura et al. (2013), expanding on the results of Segura et al. (2009), state that a metastable warm/wet climate can be attained from the impact of an 8 km-radius asteroid. Their maps do not show rain at the location of the impact itself, which is intriguingly consistent with post-3.6 Ga Mars data (Irwin et al. 2013). It is not possible to evaluate this suggestion further without additional detail on how the model was set up. Wordsworth (2016) shows that the existence of a metastable wet climate is model-dependent, and suggests that it is unlikely that the real Mars encountered a metastable wet climate state.

2. Supplementary Methods.

2.1. Obliquity Simulations.

Mars obliquity (φ) is quasi-periodic on $<10^6$ yr timescales but chaotic on $\gtrsim 10^8$ yr timescales, ranging from 0-70° (Laskar et al. 2004). These large changes have correspondingly large effects on climate (e.g. Mischna et al. 2013). φ is chaotic and cannot be deterministically reverse-integrated for times >0.1 Gyr in the past (Laskar et al. 2004). To generate realistic possible φ histories for Mars ~3 Gyr ago, we first generated an ensemble of 8-planet solar system simulations using the `mercury6` N-body code (Chambers et al. 1999). We added φ/precession tracks in postprocessing using the method of Armstrong et al. (2004). We generated randomness through 2 methods. (1) In the N-body code, we shifted Mars's position in x, y, and z at the start of the run. The positions of the other planets were left the same for all of the N-body runs. (We used JPL Horizons ephemeris for 1/1/2000 in order to ensure that the fundamental frequencies of the Solar System were the same as in the real Solar System). Although these are simulations of Mars' future, they are equally relevant to Mars' past because chaos sets in <0.1 Gyr into the run. (2) We randomly selected initial obliquities for the φ calculations from the Laskar (2004) probability distribution function.

Our runs suggest that orbital insolation alone is not a satisfactory explanation for the cadence of lake-forming climates. In our runs, the annual-maximum diurnal-mean insolation that is exceeded (at a given latitude) for 10^7 yr tends to be <20 W m^{-2} below the insolation that is exceeded for 10^4 yr (continuously) at that latitude (Fig. S3). Therefore, if direct forcing by orbitally-driven insolation is solely responsible for the variability of lake-forming climates, then olivine should be absent from catchment soils, in contradiction to observations (Fig. S3). This argument is independent of the threshold insolation for lakes, because we simply adjust the threshold insolation to match τ_1. However, the contradiction with data just described can be avoided by allowing arbitrary feedbacks – if $H2O_v$ or cirrus warming boosted the surface energy balance disproportionately during the warmest years. Another possibility is that orbitally-paced lake-forming climates create conditions that favor the sequestration of atmospheric CO_2 in carbonates (Kahn 1985, Kite et al. 2011b). Carbon sequestration would act as a brake on lake-forming climates, by increasing evaporitic cooling (Hecht 2002). In turn, this evaporitic-cooling feedback could curtail the duration and number of lake-forming climates, thus reconciling the orbital-insolation-alone hypothesis with the data. In summary, we cannot rule out the orbital-insolation hypothesis for the trigger of lake-forming climates, but our runs place constraints on an orbital-forcing explanation.

Our obliquity runs show chaotic transitions in mean φ (e.g. Armstrong et al. 2004, and references therein). Transitions are separated by long periods during which the mean φ does not vary greatly, consistent with previous work (Lissauer et al. 2012, Li & Batygin 2014). Our eccentricity pdf agrees with that of Laskar et al. (2004). Our φ pdf is unimodal, peaking at ~40°, and with a shape close to that of Laskar et al. (2004). The φ tracks show a rich structure, which is ultimately traceable to the two chaotic zones of Mars' obliquity (Laskar et al. 2004). Behaviour includes (i) abrupt, reversible drops in mean φ; (ii) abrupt, reversible spikes in mean φ; (iii) two-step increases (or decreases) in mean φ, with steps separated by 10-100 Myr; (iv) gradual ramps upward in mean-φ, and (v) a "bistability" phenomenon where Mars jumps between high mean φ and low mean φ while spending relatively little time at intermediate mean φ.

2.2. Clathrate Model.

Charge-up. Early Mars had active magmatism, initially high geothermal heat flow, a large water inventory (Villanueva et al. 2015), and a basaltic/ultramafic crust. Therefore, the amount of CH_4 produced by serpentinization early in Mars history is potentially very large (Mousis et al. 2013, Mousis et al. 2015, and references therein). Whether this potential was realized depends on the distribution of catalysts and details of crustal permeability, which are poorly known even for Earth. Our CH_4-bursts scenario requires no more than 0.0003× of the CH_4-production upper limit (from stoichiometry: ~10 bars). Because Mars crust production was extended over a long period including times during which the surface would have been cold, CH_4 produced (for example by serpentinization and Fischer-Tropsch

Type reactions; Etiope & Sherwood Lollar 2013, McCollom 2013) as crust reacted with water would have been trapped on approach to the cold surface as clathrate. CH_4 accumulates in $\sim 10^7$ yr by cycling of CH_4-saturated water through the Clathrate Hydrate Stability Zone (CHSZ), or more quickly by bubble exsolution (Tréhu et al. 2004). The extent to which pore space is filled on Mars by abiotic methane clathrate is unknown; on Earth biogenic methane clathrate fills ~3% of available pore space (Klauda & Sandler 2005).

Release. CH_4 trapped in clathrate is retained for up to Gyr. Natural-gas clathrate has SII structure. Levi et al. (2014) cite theoretical calculations by Peters et al. (2008) for which the diffusivity of CH_4 in the clathrate lattice (D_{CH4}) is given by

$$D_{CH4}(\mathrm{T}) = 0.0028 \times X_{CH4} \exp(-6.042 \times 10^{-13} / kT) \ \mathrm{cm^2\ s^{-1}}$$

For $X_{CH4} = 0.03$ (where X_{CH4} is the fraction of unoccupied cages in the clathrate lattice) and $T = 270$K (worst case for CH_4 loss) we obtain 8×10^{-16} m^2 s^{-1}. Thus in 3 Gyr, approximately 10m of clathrate will be de-methanated by CH_4 loss, which is not important for our purposes. Plausible increases to 10^{-14} m^2 s^{-1} (Root & Elwood-Madden 2012) do not alter this qualitative conclusion.

CH_4 clathrate that is moved out of the P-T range of CH_4-clathrate stability will outgas CH_4 geologically quickly (Stern et al. 2003).

We calculate CH_4-clathrate stability using a thermal model. Temperatures are calculated in each of 19 latitude bands and 400 depths using a 1D implicit scheme, using a thermal conductivity of 2.5 W m^{-1} K^{-1}. The lower boundary condition is a constant heat flux (30 mW m^{-2}). The initial condition is a geotherm in equilibrium with the annual-mean surface temperature at the first timestep. The latent heat of clathrate dissociation is ignored; this is acceptable because the thermal forcing of interest (from orbital variations) varies slowly compared to the speed of lowering of the clathrate table with or without latent-heat buffering. The upper boundary condition is an annual-mean surface temperature. This surface temperature is calculated using spin-orbit output as a function of time. The annual-mean surface temperature is the (appropriately-weighted) mean of 36 seasonal surface temperatures. The weights are proportional to the "dwell time" in that season (calculated using Kepler's equation). Each seasonal surface temperature is assumed to be in equilibrium with the diurnal mean insolation at that latitude. Insolation is a function of latitude and the time-varying spin-orbit properties calculated from the obliquity models. Obliquity and latitude are usually the most important controls. Temperatures are not permitted to fall below 169K. Calculated temperatures are uniformly increased by 30K to account for early Mars greenhouse forcing. This simple approach to greenhouse forcing is appropriate for this study because our goal is to explain runoff intermittency (not absolute temperature, not latitudinal gradients, not the existence of runoff).

The density of regolith/shallow rocks (on top of the CHSZ) is 2000 kg m^{-3}. A surface layer of 44m of ice (density 910 kg m^{-3}) is assumed poleward of 30° for $\varphi < 40°$ (Kadish et al. 2010). When $\varphi > 40°$, this ice sublimates at 1 cm yr^{-1}. This is less than the sublimation rate calculated by 3D climate models (e.g. Madeleine et al. 2009); however, faster sublimation rates would have no effect on our conclusions. Sublimation rates>0.1 cm yr^{-1} would lead to qualitatively the same conclusions. We do not include the thermal buffering of this icy material, but it would only slightly delay/damp the thermal wave. Ice-overburden sublimation tends to enhance and extend the atmosphere CH_4-enrichment episode in our model. To illustrate sensitivity to this effect, the results of a high-φ to low-φ obliquity transition are shown in Fig. S6. In this simulation ice unloading does not occur (because nontropical ice is always unstable), and methane bursts still result.

CH_4-clathrate stability zone boundaries are taken from Sloan & Koh (2008, Table 4.1). For each depth at each latitude, the code finds the first timestep (if any) at which the temperature exceeds the maximum for stability. (The code is initialized with clathrate at all depths, so there is transient degassing during model spinup, which we discard.) CH_4 destabilized is assumed to be released to the atmosphere during the same timestep. Instant release is a reasonable approximation because the thermal pulses are at orbital frequencies (10^5-10^6 yr), and – especially when fracturing associated with clathrate destabilization is taken into account – CH_4 is unlikely to be trapped for this long. Therefore any "phase lag" in the release of destabilized CH_4 is unlikely to affect our conclusions; it would simply shift the CH_4 pulses to later times by an amount almost indiscernable on our plots. Once released, CH_4 is not recharged. The amount of CH_4 released is calculated assuming porosity = 0.3 and 120 kg m^{-3} of methane for complete filling of pore space. The pore space filling factor f is a free parameter.

In our model, we do not include the effects of small amounts of C_2H_6 on the position of the CHSZ. The gas gravity estimation technique (Sloan & Koh 2008) indicates that this could shoal the CHSZ by a factor of 2-3 for $C_2H_6/CH_4 = 0.1$. Shoaling will reduce the absolute amount of gas released in our model. This is because lower $P(T)$ implies lower dP/dT; thus T increases due to orbital shifts will destabilize a reduced absolute thickness of CHSZ. However, because C_2H_6 is an effective greenhouse gas even at low concentrations, the actual warming is still likely to exceed the CH_4-only case.

Our model allows us to calculate the locations of long-term near-surface clathrate stability. Near-surface clathrates are most stable where Gyr-maximum annual-mean surface temperatures are lowest. Assuming Mars' orbital parameters have varied widely, these are 30-50°. Dusty areas, because of their high albedo and low thermal inertia, have a lower mean temperature than sandy areas or rocky areas. On Mars, the dustiest areas in the 30-50° latitude band are in the northern hemisphere. Therefore, assuming uniform charge-up of the clathrate reservoir, we predict that ancient clathrate is preserved closest to the surface in the band 30-50° N.

We do not include any feedback of CH_4-induced warming on CH_4 destabilization. Therefore, our CH_4 release amounts are conservative.

Sub-talik CH_4 release is initialized once atmospheric CH_4 exceeds an arbitrary, but radiatively reasonable (see below) threshold of 15 kg m^{-2}. We take this threshold to mark the onset of lake flooding. The talik area is set to 1.1×10^6 km^2, which is 0.7% of planet area. This could represent re-occupation of the Eridania paleolake (Irwin et al. 2002), or flooding of many smaller lakes. The depth of the warming-front is set to $2.32\sqrt{(\kappa\tau)}$ where $\kappa = 10^{-6}$ m^2 s^{-1} is diffusivity and τ is time since sub-talik release is initialized. f beneath lakes is the same as f elsewhere. All CH_4 above the warming-front is released to the atmosphere. The progress of the warming-front is halted at a depth 340 m = (2.52×10^6 Pa/(3.7 m s^{-2} × 2000 kg m^{-3})), corresponding to pressure-stabilization of CH_4-clathrate at ~277K.

2.3. CH_4 Destruction Parameterization.

The destruction of atmospheric CH_4 at high pCH_4 proceeds differently to the destruction of CH_4 at low pCH_4.

At low pCH_4, Ly-α photolysis accounts for roughly half of the CH_4 loss rate (Krasnopolsky et al. 2004). The remainder is accounted for by reactions between methane and oxidizing agents from photolysis of H_2O and CO_2 (Krasnopolsky et al. 2004). As pCH_4 increases (greater CH_4 flux), the loss due to oxidation becomes unimportant, and only photolysis matters. The hydrogen freed from CH_4 will likely escape given Mars' low gravity.

At high pCH_4 (high CH_4 flux), the photolysis loss rate is photon-limited. From Krasnopolsky et al. (2004), the Ly-α flux at Mars is ~ 4×10^{10} photons cm^{-2} s^{-1} over the disk of Mars. Therefore, the maximum CH_4 loss rate is ~4×10^{10} CH_4 molecules cm-2 s-1. For CH_4 concentrations in excess of ~1.25×10^{21} CH_4 cm^{-2} (5700 ppm for the modern atmosphere), >10^3 years are needed to remove CH_4, assuming no continuous flux from the surface.

We assume complete absorption of Ly-α. By a mean free path argument, at least $1/\sigma$ amount of CH_4 is needed for complete absorption (where σ is absorption cross section). This is (only) 5×10^{16} CH_4 cm^{-2}. "Interference" from CO_2 is unimportant when the mixing ratio of CH_4 exceeds $\sigma_{CH4}/\sigma_{CO2} = 7.4 \times 10^{-20}$ $cm^2/1.85 \times 10^{-17}$ cm^2 = 0.004 = 4000 ppm. We include CO_2 shielding of CH_4 from UV at low pCH_4 in our model. This extends the duration of the CH_4 burst, but only very slightly.

In summary, starting from a low CH_4 amount of roughly 1-10 ppb, the methane life time is ~300 years due to both photolysis and oxidation. As [CH_4] rises, the lifetime levels off at ~700 years due to photolysis alone. As methane is increased to ~0.5 %, photolysis reaches the photon limit, and CH_4 lifetime becomes proportional to CH_4 concentration. Therefore, if 1 mb of CH_4 were released into the modern Martian atmosphere due to clathrate decomposition, then it will take approximately (16 Da

/44 Da) (100 Pa/3.7 m s^{-2}) × (6 × 10^{23}/16 Da) / 4 × 10^{10} photons s^{-1}/(86400 s × 365 × 10^3) ~ 30 Kyr to eliminate.

C_2H_6 has σ ~ 2.5 × 10^{-17} cm^2 $molecule^{-1}$ (Keller-Rudek et al. 2013), so at 10% abundance C_2H_6 has a photolysis lifetime similar to CH_4. Photochemical *production* of C_2H_6 is small until the CH_4/CO_2 ratio reaches values higher than those considered in this study (Wong et al. 2003).

The Ly-α flux as a function of star age was calculated using Güdel (2007) and Ribas et al. (2005):

I_{1216} = (3.7×10^{-11} cm^{-2} s^{-1}) × $t_{Gyr}^{-0.72}$/ $4.56^{-0.72}$

where t_{Gyr} is the time after Mars formation in Gyr. The underlying dataset of Ly-α flux from Solar-analog stars has no data points between star age 0.65 Gyr and star age 4.56 Gyr (Ribas et al. 2005). Plausible variations in the scaling (and incorporation of absorption of UV by CH_4 outside the main Ly-α band) could affect the CH_4 lifetime by a factor of 2-3.

2.4 Radiative Model.

We use a 1D radiative model representing a low-latitude, warm-season atmospheric column. Our temperature profiles are set by patching an adiabat to an isothermal 165K stratosphere with surface temperature 273K. The temperature profiles are fixed and do not adjust with CH_4 amount. Whilst absorption by high CH_4 can cause a stratospheric temperature inversion in nitrogen based atmospheres, high CO_2 (the background gas here) prevents that due to strong 15-μm emission (Byrne & Goldblatt, 2015). Indeed, the assumption of an isothermal stratosphere is likely conservative given the CO2 background, and radiative warming may be higher than calculated. The radiative transfer is performed with the SMART code (written by David Crisp), which operates at line-by-line resolution, using HITRAN 2012 line data (Rothman et al. 2013). This method directly follows Byrne & Goldblatt (2014), but uses planetary parameters applicable for early Mars.

Example clear-sky results (for CH_4 + CO_2) are shown in Figs. S3-S6 (for upwelling radiation at the top of the atmosphere). At low pCO_2 and negligible CH_4 mixing ratio, the only greenhouse effect is the CO_2 15-μm band. At low pCO_2 and high CH_4, this warming is supplemented by 8-μm absorption by CH_4. As CO_2 increases, CO_2 and CH_4 start to compete for the same spectral lines, so the warming effect of CH_4 is reduced. Net warming by CH_4 is also reduced by solar absorption in the near-infrared (Byrne & Goldblatt 2015). The solar absorption effect is slightly worse for the redder young Sun, an effect that we ignore. Our radiative model does not include greenhouse warming by cirrus clouds, which could be important in setting the pre-peturbation energy balance (Ramirez & Kasting 2016), but would only reduce the net CH_4 forcing by 14-30%. We do not include *T-P* profile adjustment to CH_4 forcing, because this adjustment depends on the mechanism for background warming (e.g., cloud decks versus well-mixed gases) and this mechanism is not known. We also do

not include CH_4-CO_2 collision-induced absorption (Wordsworth et al. 2016), which is strongest at high pCO_2, and which provides an alternative channel for CH_4-triggered warming.

CH_4-triggered lake-forming climate requires that surface temperature (*T*) before CH_4 is released is relatively warm. One reason is that the direct (no feedbacks) radiative forcing of CH_4 is insufficient by itself to warm early Mars to the melting point (e.g. Forget et al. 2013, Wordsworth et al. 2015). Additionally, the principal CH_4 band is at 8 μm, so Mars must be warm enough for the surface to radiate significantly at 8 μm in order for CH_4 to have radiative forcing. Finally, the minimum CHSZ pressure increases log-linearly with *T*. Therefore, at higher initial *T*, a unit increase in *T* will destabilize a larger absolute depth range of CH_4 clathrate (and so release more CH_4 to the atmosphere) than at lower *T*.

This sensitivity to initial *T* is reduced for C_2H_6 warming, because the principal absorption band of C_2H_6 (12.5 μm) band is closer to the center of Mars' Planck function (Byrne & Goldblatt 2014).

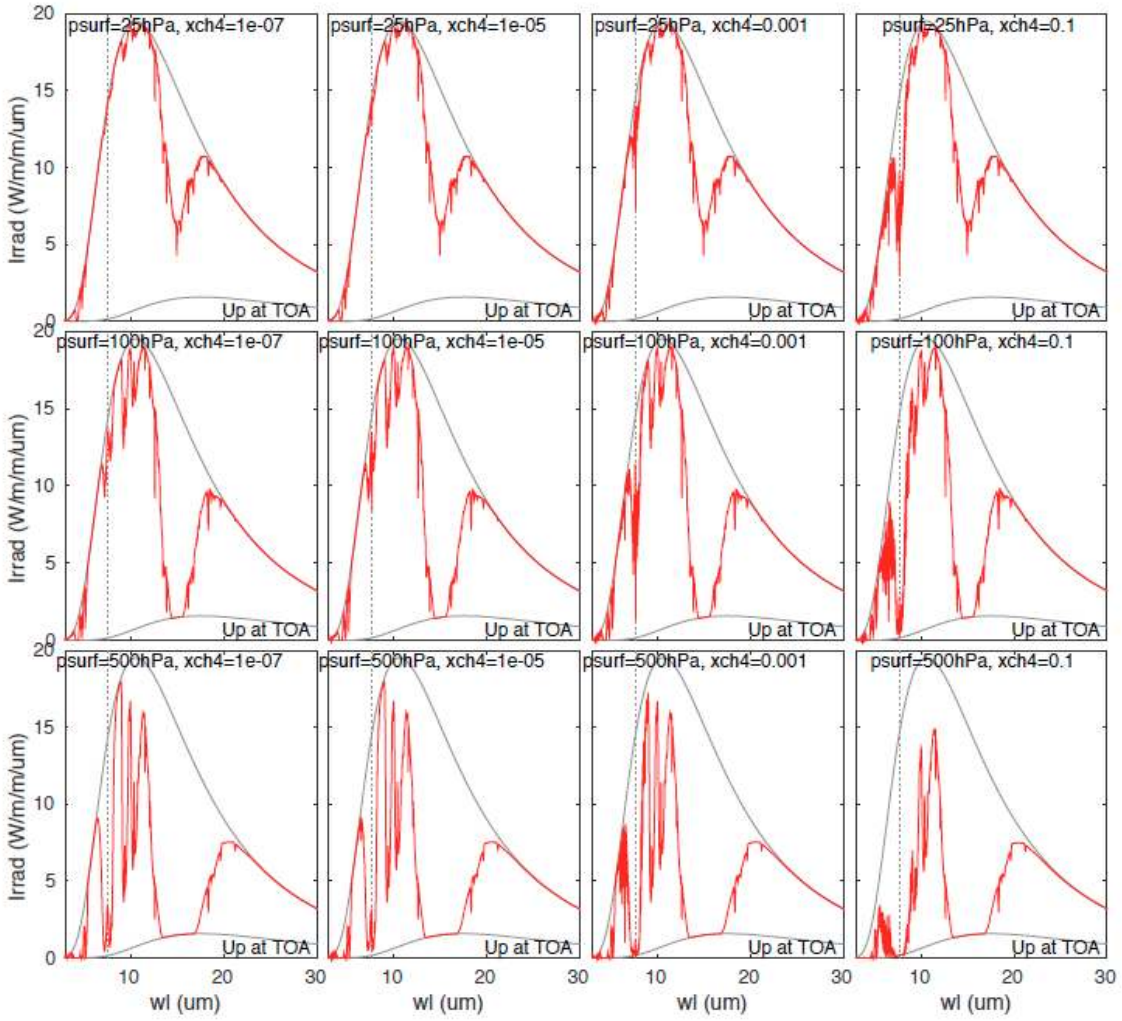

Fig. S2. Outgoing Longwave Radiation at the Top Of Atmosphere (TOA) assuming a 273K surface, 165K isothermal stratosphere, and varying amounts of atmospheric CO_2 ("psurf") and varying CH_4 volume mixing ratio ("xch4"). Grey lines are the Plank functions for the surface and stratosphere temperatures. The position of the main CH_4 absorption band is shown with a vertical dotted line.

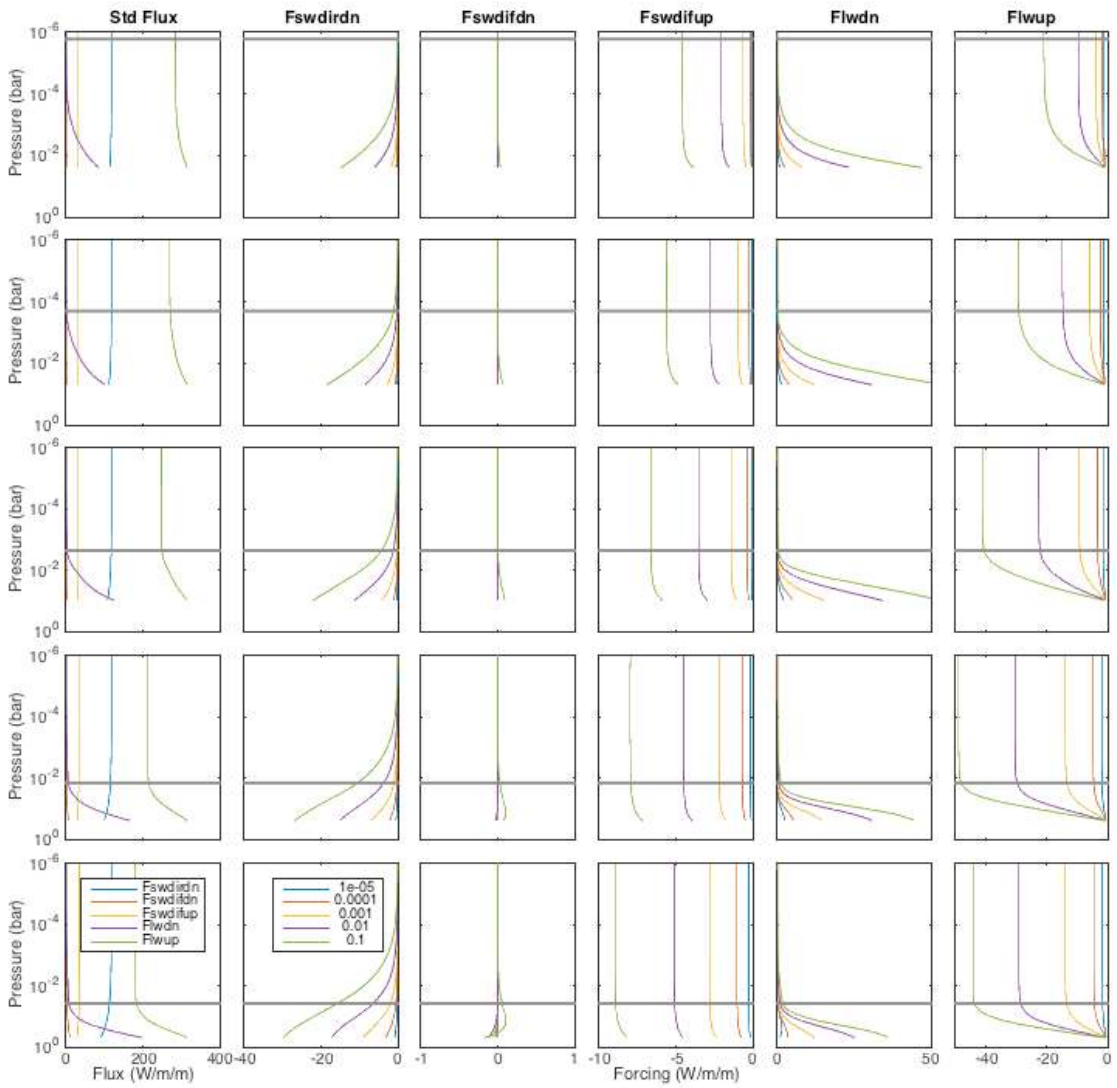

Fig. S3. Effect of CH_4 on Mars atmosphere radiative fluxes. 273K surface temperature, adiabatic troposphere, isothermal 165K stratosphere. Rows correspond to increasing pCO2: {25 mbar, 50 mbr, 100 mbar, 250 mbar, 500 mbar}. Grey bar = tropopause. Left column = Fluxes in the zero-CH_4 case ("Std Flux"). "Fswdirdn" = Flux of shortwave direct radiation, downwelling. "Fswdifdn" = Flux of shortwave diffuse radiation, downwelling. "Fswdifup" = Flux of shortwave diffuse radiation, upwelling. "Flwdn" = Flux of longwave radiation, downwelling. "Flwup" = Flux of longwave radiation, upwelling.

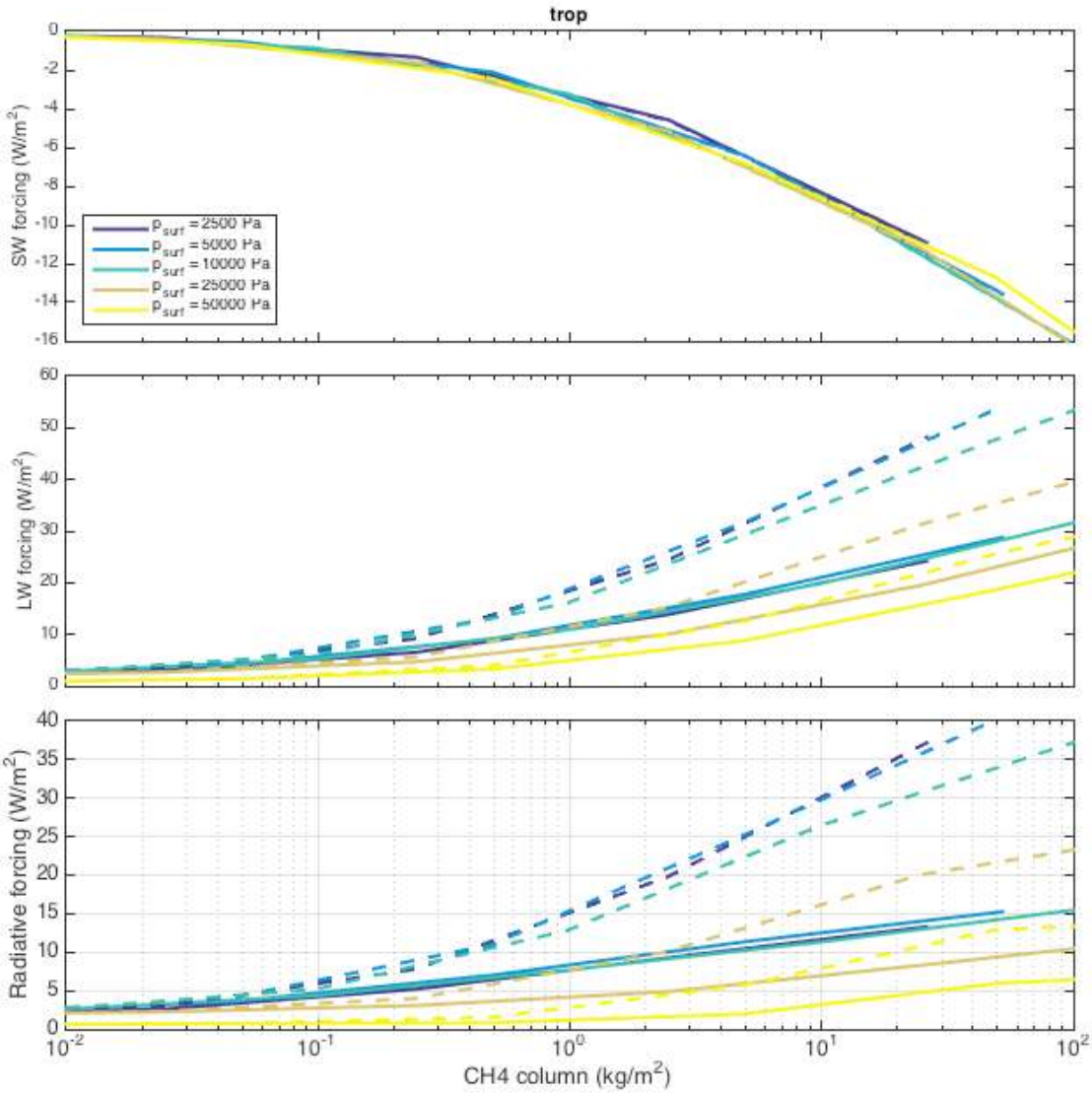

Fig. S4. Tropopause forcing for (solid lines) CH_4 only, and (dashed lines) CH_4 + 10% C_2H_6. Colors correspond to total atmospheric pressures.

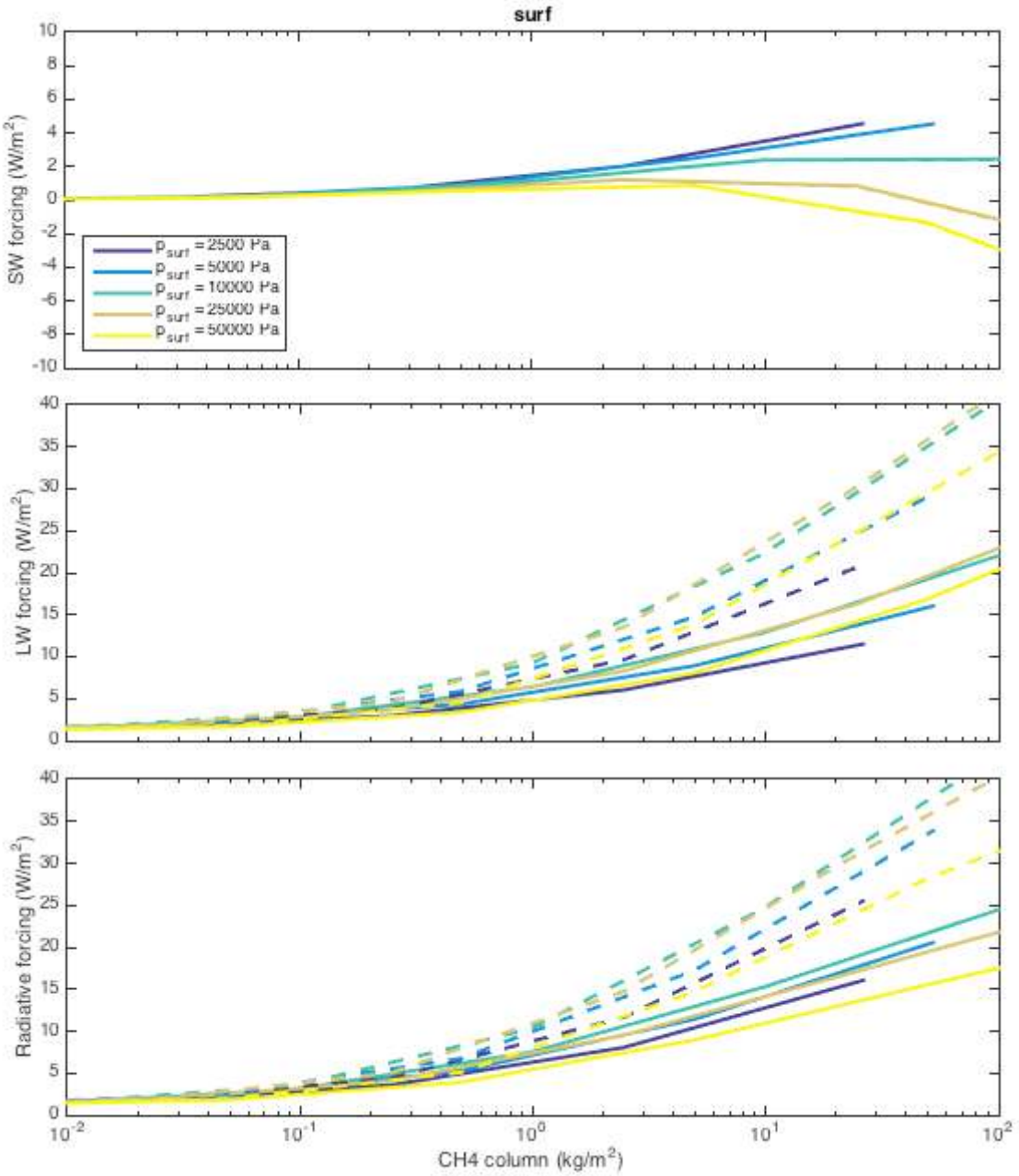

Fig. S5. Surface forcing for (solid lines) CH_4 only, and (dashed lines) CH_4 + 10% C_2H_6. Colors correspond to total atmospheric pressures.

2.5. Possible Climate Feedbacks.

A one-equation model suggests that a warmer Early Mars would have a high climate sensitivity. In the optically thick limit appropriate to Early Mars, for a gray-gas all-troposphere atmosphere, top-of-the-atmosphere energy balance G is given by (Pierrehumbert 2010)

$$G = \text{OLR} - \text{ISR} = (\sigma T_s^4 \, \tau_\infty^{-4R/Cp} \, \Gamma) - \text{ISR} = 0 \qquad (3)$$

where OLR is outgoing longwave radiation, ISR is absorbed shortwave radiation, σ is the Stefan-Boltzmann constant, T_s is surface temperature, τ_∞ is optical depth, and Γ is a constant (≈0.97 for pure CO_2). $(4R/Cp) \approx 1$ for CO_2. Solving for an Early Mars at 270K adopting standard solar-brightening models and an overall planet albedo 0.2, $\tau_\infty \approx 4$, so the optically thick limit is justified a posteriori. Rearranging and differentiating (3) to find dT_s/dG, $\tau_\infty \approx 4$ gives ~0.8 K W^{-1} m^2 climate sensitivity. Now consider a hypothetical planet at 270K, with a weak (optically thin) greenhouse. For this weak-greenhouse planet, an imposed change in the top-of-the-atmosphere energy balance will produce modest warming due to Planck feedback (~0.2 K W^{-1} m^2). Therefore a warmer early Mars is also more sensitive to climate feedbacks - 4× more sensitive in this toy-model example.

The main text discusses feedbacks. Here we discuss two additional relevant points:

- The cause of the "background" warming needed to explain a warmer Early Mars climate state is unknown. This "background" warming could be enhanced by CH_4 warming, as discussed (for the one-equation model atmosphere) above. Alternatively, CH_4 warming could weaken the background forcing, for example by dispersing clouds or reducing the grain-size of clouds; a negative feedback. Background warming would also compete for spectral lines. This would weaken initial radiative forcing, but the main candidate mechanisms for background warming either have broad absorptions, or spectral bands without important overlaps with CH_4 (Byrne & Goldblatt 2014, Wordsworth 2016.)

- Groundwater outbursts could be triggered by, or themselves initiate, CH_4-induced radiative forcing. For example, the volume change associated with clathrate dissociation might create the high-permability fractures that are necessary to explain chaos-terrain hydrographs (Harrison & Grimm 2008, Hanna & Phillips 2007).

(a)

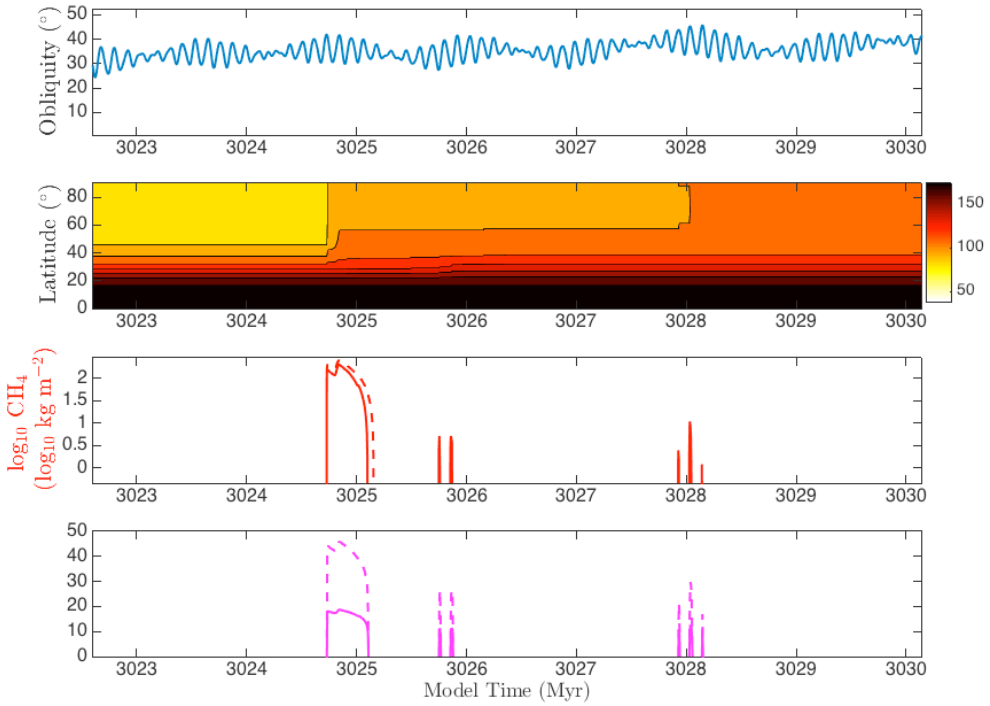
Obliquity (°)
Latitude (°)
log10 CH4 (log10 kg m−2)
Model Time (Myr)

(b)

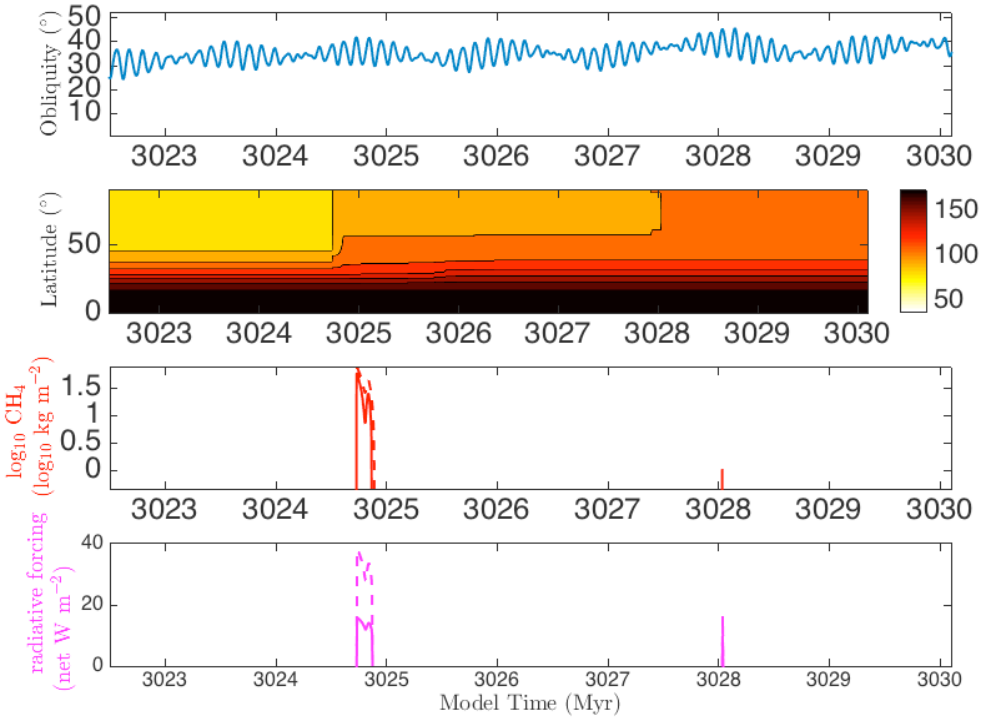
Obliquity (°)
Latitude (°)
log10 CH4 (log10 kg m−2)
radiative forcing (net W m−2)
Model Time (Myr)

(c)

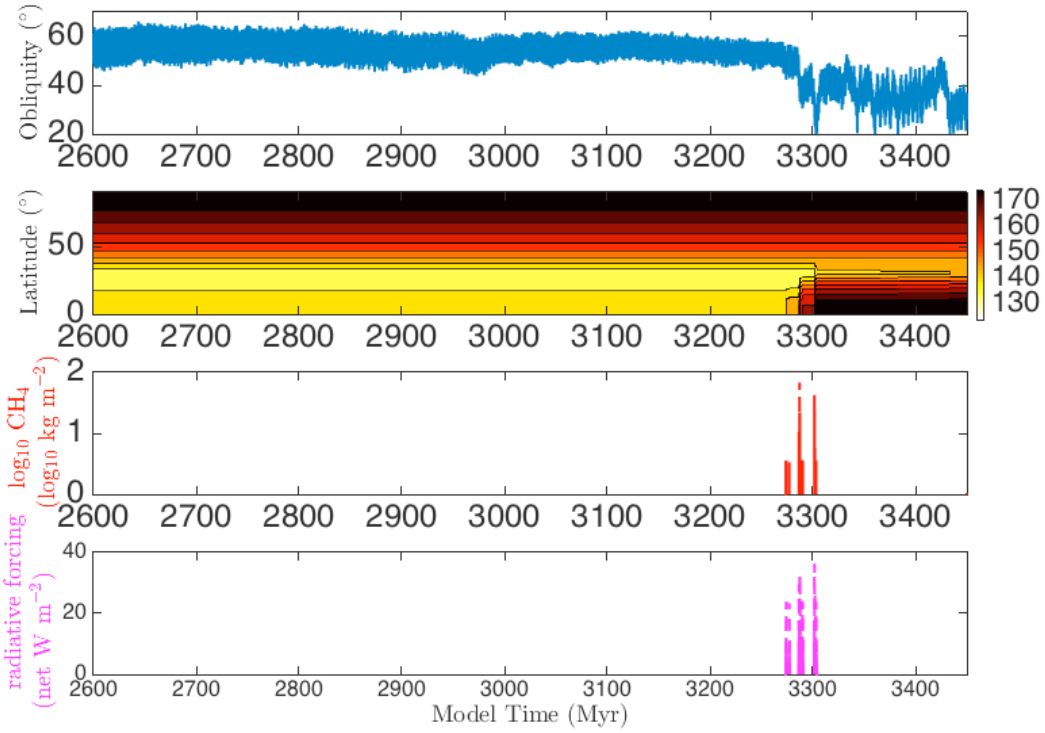
Obliquity (°)
60
40
20
2600 2700 2800 2900 3000 3100 3200 3300 3400
Latitude (°)
50
0
170
160
150
140
130
log10 CH4 (log10 kg m−2)
2
1
0
radiative forcing (net W m−2)
40
20
0
Model Time (Myr)

(d)

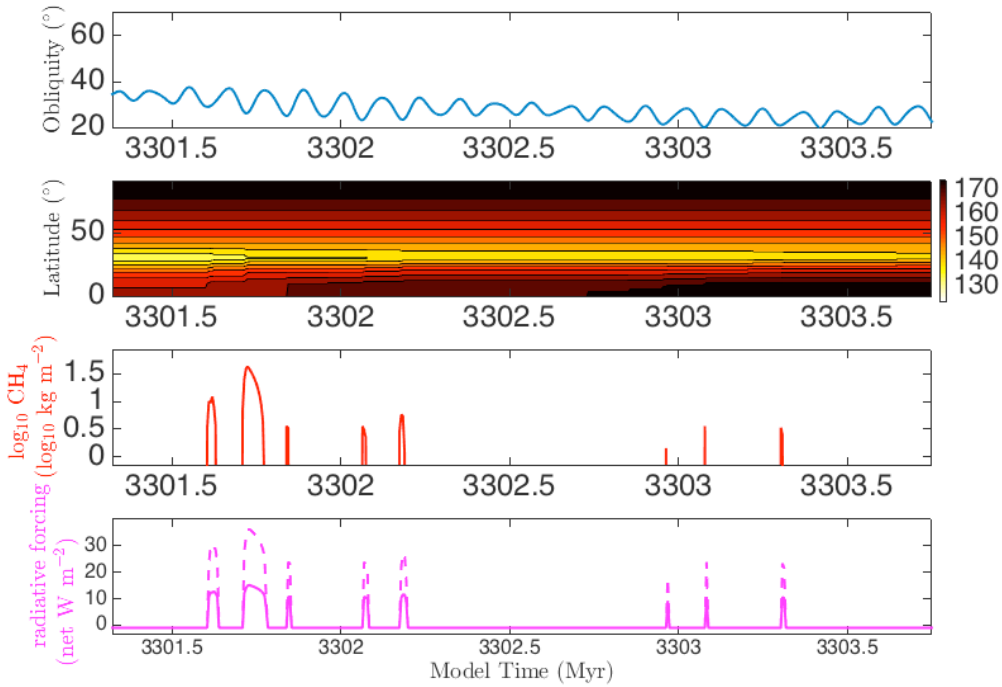
Obliquity (°)
60
40
20
3301.5 3302 3302.5 3303 3303.5
Latitude (°)
50
0
170
160
150
140
130
log10 CH4 (log10 kg m−2)
1.5
1
0.5
0
radiative forcing (net W m−2)
30
20
10
0
Model Time (Myr)

(e)

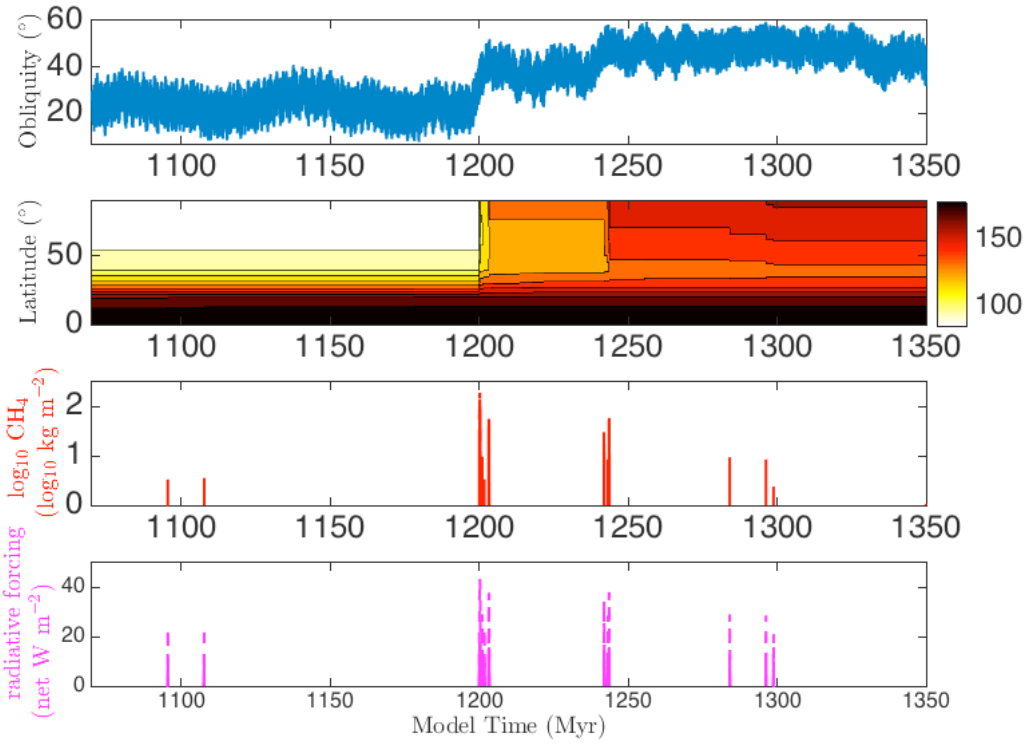
Obliquity (°)
60
40
20
1100
1150
1200
1250
1300
1350
Latitude (°)
50
0
150
100
log10 CH4 (log10 kg m−2)
2
1
0
radiative forcing (net W m−2)
40
20
0
Model Time (Myr)

(f)

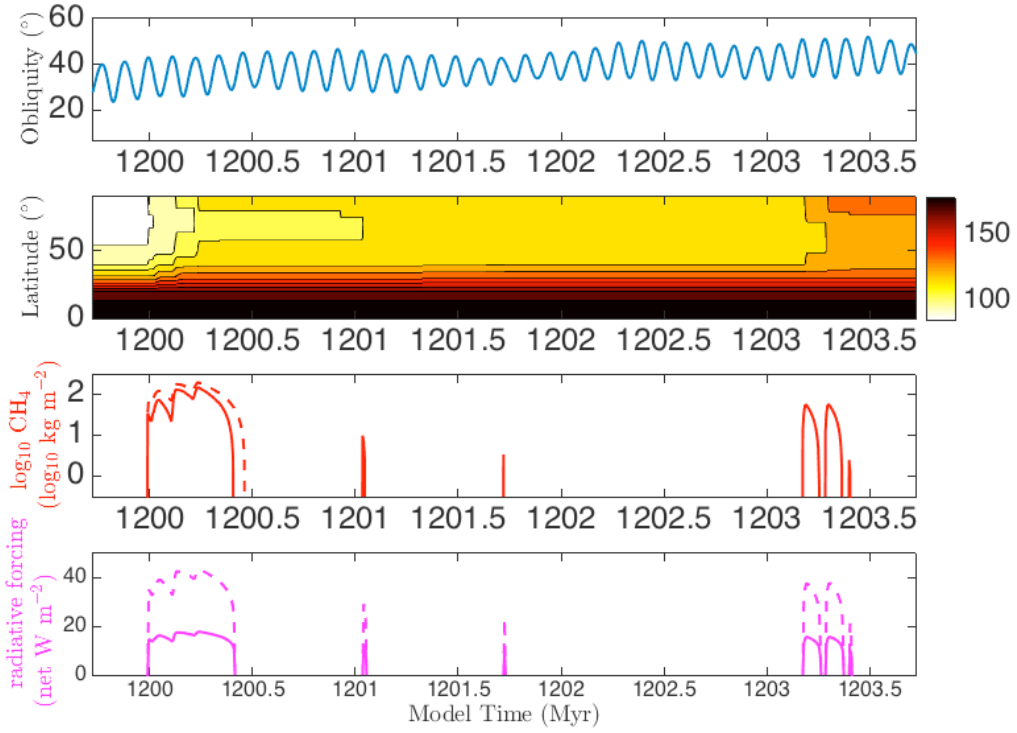
Obliquity (°)
60
40
20
1200
1200.5
1201
1201.5
1202
1202.5
1203
1203.5
Latitude (°)
50
0
150
100
log10 CH4 (log10 kg m−2)
2
1
0
radiative forcing (net W m−2)
40
20
0
Model Time (Myr)

Fig. S6. Different CH_4-release scenarios. For each subfigure, the top panel shows example obliquity forcing. The colors in the second panel show the depth to the top of the clathrate-hydrate stability zone (depth in meters). Darkening of colors indicates clathrate destabilization. The third panel shows atmospheric CH_4 column mass. Dashed line includes talik feedback. The bottom panel shows radiative forcing, without any climate feedbacks. Solid line is for CH_4 alone; dashed line is for CH_4+10%C_2H_6. (a) Zoom in on the biggest CH_4 burst from the simulation shown in Fig. 4. (b) As for (a), but with f = 0.2. (c) CH_4 bursts for a simulation of long-term φ decline (temperature effects only, no decompression). (d) Zoom in on part of (c). (e) Showing another φ-rise scenario (compare to Fig. 4). (f) Zoom in on the biggest CH_4 burst from the simulation shown in (e).

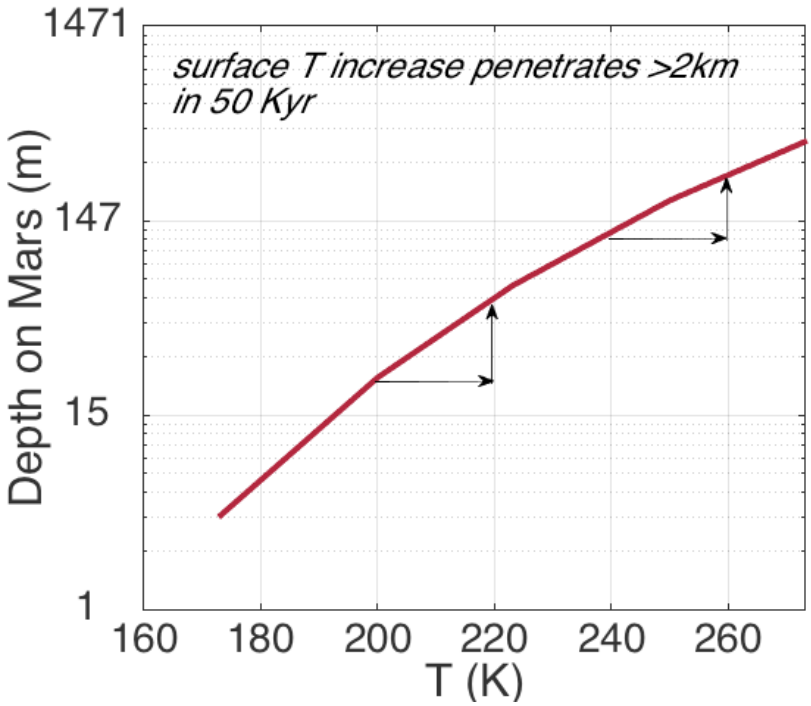

Fig. S7. Methane clathrate hydrate is stable at low temperature and high pressure (red line shows phase boundary). Arrows show that for a given temperature increase, the absolute change in depth to the top of the Clathrate Hydrate Stability Zone (CHSZ) is greater at high temperature.

Supplementary References.

Adeli, Solmaz; Hauber, Ernst; Kleinhans, Maarten; Le Deit, Laetitia; Platz, Thomas; Fawdon, Peter; Jaumann, Ralf, 2016, Amazonian-aged fluvial system and associated ice-related features in Terra Cimmeria, Mars, Icarus, 277, 286-299.

Armstrong, J.C., Barnes, R., Domagal-Goldman, S., Breiner, J., Quinn, T.R., Meadows, V.S. 2014. Effects of Extreme Obliquity Variations on the Habitability of Exoplanets. Astrobiology 14, 277-291.

Baker, D.M.H., Head, J.W. 2015. Extensive Middle Amazonian mantling of debris aprons and plains in Deuteronilus Mensae, Mars: Implications for the record of mid-latitude glaciation. Icarus 260, 269-288.

Barnhart, C.J., Howard, A.D., Moore, J.M. 2009. Long-term precipitation and late-stage valley network formation: Landform simulations of Parana Basin, Mars. JGR (Planets) 114, E01003.

Berger, G., et al., 2009, Evidence in favor of small amounts of ephemeral and transient water during alteration at Meridiani Planum, Mars, American Mineralogist, 94, pages 1279–1282, 2009.

Byrne, B.; Goldblatt, C., 2015, Diminished greenhouse warming from Archean methane due to solar absorption lines, Climate of the Past, 11, 559-570.

Chambers, J.E. 1999. A hybrid symplectic integrator that permits close encounters between massive bodies. Monthly Notices of the Royal Astronomical Society 304, 793-799.

Dietrich, WE, Palucis MC, Williams RME, Lewis KW, Rivera-Hernandez F, and Sumner DY, Fluvial gravels on Mars: Analysis and implications, accepted, Gravel-Bed Rivers 8.

Ehlmann, B.L., Buz, J. 2015. Mineralogy and fluvial history of the watersheds of Gale, Knobel, and Sharp craters. Geophys. Res. Lett. 42, 264-273.

Etiope, G., Sherwood Lollar, B. 2013. Abiotic Methane on Earth. Reviews of Geophysics 51, 276-299.

Etiope, G.; Ehlmann, B.L.; Schoell, M., 2013, Low temperature production and exhalation of methane from serpentinized rocks on Earth: A potential analog for methane production on Mars, Icarus, 224, 2, p. 276-285.

Fassett, C.I., Head, J.W. 2008. The timing of martian valley network activity: Constraints from buffered crater counting. Icarus 195, 61-89.

Forget, F., Haberle, R.M., Montmessin, F., Levrard, B., Head, J.W. 2006. Formation of Glaciers on Mars by Atmospheric Precipitation at High Obliquity. Science 311, 368-371.

Grant, J.A., Wilson, S.A. 2011. Late alluvial fan formation in southern Margaritifer Terra, Mars. Geophys. Res. Lett. 38, L08201.

Grant, J.A., Wilson, S.A. 2012. A possible synoptic source of water for alluvial fan formation in southern Margaritifer Terra, Mars. Planet. and Space Sci. 72, 44-52.

Grant, J.A., Wilson, S.A., Mangold, N., Calef, F., Grotzinger, J.P. 2014. The timing of alluvial activity in Gale crater, Mars. Geophys. Res. Lett. 41, 1142-1149.

Hanna, J.C.A. & Phillips, R. 2007, Hydrological modeling of outflow channels and chaos regions on Mars, Journal of Geophysical Research, Volume 112, Issue E8, CiteID E08001.

Harrison & Grimm, 2008, Multiple flooding events in Martian outflow channels, Journal of Geophysical Research, Volume 113, Issue E2, CiteID E02002.

Hauber, E., Platz, T., Reiss, D., Le Deit, L., Kleinhans, M.G., Marra, W.A., Haas, T., Carbonneau, P. 2013. Asynchronous formation of Hesperian and Amazonian-aged deltas on Mars and implications for climate. JGR (Planets) 118, 1529-1544.

Hecht, Michael H., 2002, Metastability of Liquid Water on Mars, Icarus, 156, 2, 373-386.

Hoke, Monica R. T.; Hynek, Brian M. (2009), Roaming zones of precipitation on ancient Mars as recorded in valley networks, J. Geophys. Res., 114, E8, CiteID E08002.

Howard, A.D., Moore, J.M. 2011. Late Hesperian to early Amazonian midlatitude Martian valleys: Evidence from Newton and Gorgonum basins. JGR (Planets) 116, E05003.

Hurowitz, Joel A.; McLennan, Scott M., 2007, A ~3.5 Ga record of water-limited, acidic weathering conditions on Mars, Earth and Planetary Science Letters, 260, Issue 3-4, p. 432-443.

Irwin, R.P., III, Craddock, R.A., Howard, A.D. 2005. Interior channels in Martian valley networks: Discharge and runoff production. Geology 33, 489.

Irwin, R.P., III, 2013. Testing Links Between Impacts and Fluvial Erosion on Post-Noachian Mars, Lunar and Planetary Science Conference, LPI Contribution No. 1719, p.2958.

Kahn, R., 1985, The evolution of CO2 on Mars, Icarus, vol. 62, May 1985, p. 175-190.

Keller-Rudek, H., Moortgat, G. K., Sander, R., and Sörensen, R., 2013, The MPI-Mainz UV/VIS spectral atlas of gaseous molecules of atmospheric interest, Earth Syst. Sci. Data, 5, 365–373.

Kite, E.S., Michaels, T.I., Rafkin, S., Manga, M., Dietrich, W.E. 2011a, Localized precipitation and runoff on Mars. JGR (Planets) 116, E07002.

Kite, E.S.; Gaidos, E.; Manga, M., 2011b, Climate Instability on Tidally Locked Exoplanets, Astrophys. J., 743, 41.

Kite, E.S., Halevy, I., Kahre, M.A., Wolff, M.J., Manga, M. 2013. Seasonal melting and the formation of sedimentary rocks on Mars, with predictions for the Gale Crater mound. Icarus 223, 181-210.

Klauda, J.B., and Sandler, S.I., 2005, Global Distribution of Methane Hydrate in Ocean Sediment, Energy Fuels, 19 (2), 459–470.

Koeppen, W.C., Hamilton, V.E. 2008. Global distribution, composition, and abundance of olivine on the surface of Mars from thermal infrared data. JGR (Planets) 113, E05001.

Komatsu, G., Okubo, C.H., Wray, J.J., Ojha, L., Cardinale, M., Murana, A., Orosei, R., Chan, M.A., Örmo, J., Gallagher, R. 2016. Small edifice features in Chryse Planitia, Mars: Assessment of a mud volcano hypothesis. Icarus 268, 56-75.

Lamb, M.P.; Dietrich, W.E.; Aciego, S.M.; DePaolo, D.J.; Manga, M., 2008, Formation of Box Canyon, Idaho, by Megaflood: Implications for Seepage Erosion on Earth and Mars, Science, 320, 5879, 1067-.

Levi, A.; Sasselov, D.; Podolak, M. (2014), Structure and Dynamics of Cold Water Super-Earths: The Case of Occluded CH4 and Its Outgassing, The Astrophysical Journal, 792, 2, article id. 125, 44 pp.

Li, G., Batygin, K. 2014. On the Spin-axis Dynamics of a Moonless Earth. Astrophys. J. 790, 69.

Lissauer, J.J., Barnes, J.W., Chambers, J.E. 2012. Obliquity variations of a moonless Earth. Icarus 217, 77-87.

Lillis, R. J.; Brain, D. A.; Bougher, S. W.; Leblanc, F.; Luhmann, J. G.; Jakosky, B. M.; Modolo, R.; Fox, J.; Deighan, J.; Fang, X.; Wang, Y. C.; Lee, Y.; Dong, C.; Ma, Y.; Cravens, T.; Andersson, L.; Curry, S. M.; Madeleine, J.-B., Forget, F., Head, J.W., Levrard, B., Montmessin, F., Millour, E. 2009. Amazonian northern mid-latitude glaciation on Mars: A proposed climate scenario. Icarus 203, 390-405.

Mahaffy, P.R., and 27 colleagues 2015. The imprint of atmospheric evolution in the D/H of Hesperian clay minerals on Mars. Science 347, 412-414.

Mangold, N., Adeli, S., Conway, S., Ansan, V., Langlais, B. 2012. A chronology of early Mars climatic evolution from impact crater degradation. JGR (Planets) 117, E04003.

Mangold, N., Quantin, C., Ansan, V., Delacourt, C., Allemand, P. 2004. Evidence for Precipitation on Mars from Dendritic Valleys in the Valles Marineris Area. Science 305, 78-81.

McLennan, S., et al., 2014, Elemental Geochemistry of Sedimentary Rocks at Yellowknife Bay, Gale Crater, Mars, Science, Volume 343, Issue 6169, id. 1244734 (2014).

Mischna, M.A., Richardson, M.I., Wilson, R.J., McCleese, D.J. 2003. On the orbital forcing of Martian water and CO_2 cycles: A general circulation model study with simplified volatile schemes. JGR (Planets) 108, 5062-1.

Morgan, A.M., Howard, A.D., Hobley, D., Moore, J.M., Dietrich, W.E., Williams, R.M.E., Burr, D.M., Grant, J.A., Wilson, S.A., Matsubara, Y. 2014. Sedimentology and climatic environment of alluvial fans in the martian Saheki crater & comparison with terrestrial fans in the Atacama Desert. Icarus 229, 131-156.

Mousis, O., and 10 colleagues 2013. Volatile Trapping in Martian Clathrates. Space Science Reviews 174, 213-250.

Mousis, O., and 10 colleagues 2015. Methane Clathrates in the Solar System. Astrobiology 15, 308-326.

Ody, A., Poulet, F., Bibring, J.-P., Loizeau, D., Carter, J., Gondet, B., Langevin, Y. 2013. Global investigation of olivine on Mars. JGR (Planets) 118, 234-262.

Palucis, M.C., Dietrich, W.E., Hayes, A.G., Williams, R.M.E., Gupta, S., Mangold, N., Newsom, H., Hardgrove, C., Calef, F., Sumner, D.Y. 2014. The origin and evolution of the Peace Vallis fan system that drains to the Curiosity landing area, Gale Crater, Mars. JGR (Planets) 119, 705-728.

Palucis, M.C., Dietrich, W.E., Williams, R.M.E., Hayes, A.G., Parker, T., Sumner, D.Y., Mangold, N., Lewis, K., Newsom, H. 2016. Sequence and relative timing of large lakes in Gale crater (Mars) after the formation of Mount Sharp. JGR (Planets) 121, 472-496.

Peters, B., Zimmermann, N.E.R., Beckham, G.T., Tester, J.W., Trout, B.L., 2008. Path sampling calculation of methane diffusivity in natural gas hydrates from a water-vacancy assisted mechanism. J. Am. Chem. Soc. 130, 17,342–17,350.

Pierrehumbert, R., 2010, Principles of planetary climate, Cambridge University Press.

Ramirez, Ramses M.; Kasting, James F. (2016), Could Cirrus Clouds Have Warmed Early Mars?, arXiv:1608.03891, accepted for publication in Icarus.

Ribas, I., Guinan, E.F., Güdel, M., Audard, M. 2005. Evolution of the Solar Activity over Time and Effects on Planetary Atmospheres. I. High-Energy Irradiances. Astrophysical Journal 622, 680-694.

Robbins, S.J. 2014. New crater calibrations for the lunar crater-age chronology. Earth and Planetary Science Letters 403, 188-198.

Rothman, L.S., I. E. Gordon, Y. Babikov et al., 2013, The HITRAN 2012 Molecular Spectroscopic Database, Journal of Quantitative Spectroscopy and Radiative Transfer 130, 4-50.

Segura, T.L., & Colaprete, A, 2009, Global Modeling of Impact-induced Greenhouse Warming on Early Mars, 40th Lunar and Planetary Science Conference, (Lunar and Planetary Science XL), held March 23-27, 2009 in The Woodlands, Texas, id.1056.

Segura, T.L., et al. 2013, The Effects of Impacts on the Climates of Terrestrial Planets, in Comparative Climatology of Terrestrial Planets, Stephen J. Mackwell, Amy A. Simon-Miller, Jerald W. Harder, and Mark A. Bullock (eds.), University of Arizona Press, Tucson, 610 pp., p.417-437

Shean, D.E. 2010. Candidate ice-rich material within equatorial craters on Mars. Geophys. Res. Lett. 37, L24202.

Sholes, S.F., M.L. Smith, M.W. Claire, K.J. Zahnle, and D.C. Catling., 2015, An Anoxic Atmosphere on Early, Volcanically Active Mars and its Implications for Life. Astrobiology Sci. Conf., Abs. #7455.

Sloan, E.D., & Koh, C.A., 2008, Clathrate Hydrates of Natural Gases (3rd Edition), CRC Press.

Skinner, J.A., Tanaka, K.L., Platz, T. 2012. Widespread loess-like deposit in the Martian northern lowlands identifies Middle Amazonian climate change. Geology 40, 1127-1130.

Som, S.M., Montgomery, D.R., Greenberg, H.M. 2009. Scaling relations for large Martian valleys. JGR (Planets) 114, E02005.

Stern, L.A., Circone, S., Kirby, S.H., Durham, W.B. 2003. Temperature, pressure, and compositional effects on anomalous or ''self'' preservation of gas hydrates. Canadian Journal of Physics 81, 271-283.

Tosca, N.J., Knoll, A.H. 2009. Juvenile chemical sediments and the long term persistence of water at the surface of Mars. Earth and Planetary Science Letters 286, 379-386.

Tréhu, Anne M.; Flemings, Peter B.; Bangs, Nathan L.; Chevallier, Johanna; Gràcia, Eulàlia; Johnson, Joel E.; Liu, C.-S.; Liu, Xiaoli; Riedel, Michael; Torres, Marta E., 2014, Feeding methane vents and gas hydrate deposits at south Hydrate Ridge, Geophysical Research Letters, Volume 31, Issue 23, CiteID L23310.

Villanueva, G. L.; Mumma, M. J.; Novak, R. E.; Käufl, H. U.; Hartogh, P.; Encrenaz, T.; Tokunaga, A.; Khayat, A.; Smith, M. D., 2015, Strong water isotopic anomalies in the martian atmosphere: Probing current and ancient reservoirs, Science, 348, 218-221.

Viviano-Beck, C.E., and 10 colleagues 2014. Revised CRISM spectral parameters and summary products based on the currently detected mineral diversity on Mars. JGR (Planets) 119, 1403-1431.

Warner, N., Gupta, S., Kim, J.-R., Lin, S.-Y., Muller, J.-P. 2010. Hesperian equatorial thermokarst lakes in Ares Vallis as evidence for transient warm conditions on Mars. Geology 38, 71-74.

Werner, S.C., Tanaka, K.L. 2011. Redefinition of the crater-density and absolute-age boundaries for the chronostratigraphic system of Mars. Icarus 215, 603-607.

Wilson, Sharon A., Alan D. Howard, Jeffrey M. Moore, John A. Grant (2016), A Cold-Wet Mid-Latitude Environment on Mars during the Hesperian-Amazonian Transition: Evidence from Northern Arabia Valleys and Paleolakes, J. Geophys. Res. Planets, accepted manuscript, DOI: 10.1002/2016JE005052

Woo, M.-K., 2012, Permafrost Hydrology, Springer.

Wong, Ah-San; Atreya, Sushil K.; Encrenaz, Thérèse, 2003, Chemical markers of possible hot spots on Mars, J. Geophys. Res. (Planets), 108, Issue E4, pp. 7-1, CiteID 5026.

Williams, R.M.E., Malin, M.C. 2008. Sub-kilometer fans in Mojave Crater, Mars. Icarus 198, 365-383.

Williams, R., Rogers, A.D., Chojnacki, M., Boyce, J., Seelos, K., Hardgrove, C., Chuang, F. 2011. Evidence for episodic alluvial fan formation in far western Terra Tyrrhena, Mars. Icarus 211, 222-237.

Wordsworth, R., Forget, F., Millour, E., Head, J.W., Madeleine, J.-B., Charnay, B. 2013. Global modelling of the early martian climate under a denser CO_2 atmosphere: Water cycle and ice evolution. Icarus 222, 1-19.

Wordsworth, R., 2016, The Climate of Early Mars, Annual Reviews of Earth and Planetary Sciences.